2010

Mergers, Active Galactic Nuclei and Normal Galaxies: Contributions to the Distribution of Star Formation Rates and Infrared Luminosity Functions

P. F. Hopkins

J. D. Younger

C. C. Hayward

Desika Narayanan
Haverford College, dnarayan@haverford.edu

Monthly Notices
of the
ROYAL ASTRONOMICAL SOCIETY

Mon. Not. R. Astron. Soc. **402,** 1693–1713 (2010) doi:10.1111/j.1365-2966.2009.15990.x

Mergers, active galactic nuclei and 'normal' galaxies: contributions to the distribution of star formation rates and infrared luminosity functions

Philip F. Hopkins,[1⋆] Joshua D. Younger,[2†] Christopher C. Hayward,[3] Desika Narayanan[3] and Lars Hernquist[3]

[1]*Department of Astronomy and Theoretical Astrophysics Center, University of California Berkeley, Berkeley, CA 94720, USA*
[2]*Institute for Advanced Study, Einstein Drive, Princeton, NJ 08540, USA*
[3]*Harvard–Smithsonian Center for Astrophysics, 60 Garden Street, Cambridge, MA 02138, USA*

Accepted 2009 November 4. Received 2009 October 23; in original form 2009 September 17

ABSTRACT

We use a novel method to predict the contribution of normal star-forming galaxies, merger-induced bursts and obscured active galactic nuclei (AGN), to infrared luminosity functions (LFs) and global star formation rate (SFR) densities. We use empirical halo occupation constraints to populate haloes with galaxies and determine the distribution of normal and merging galaxies. Each system can then be associated with high-resolution hydrodynamic simulations. We predict the distribution of observed luminosities and SFRs, from different galaxy classes, as a function of redshift from $z = 0$ to 6. We provide fitting functions for the predicted LFs, quantify the uncertainties, and compare with observations. At all redshifts, 'normal' galaxies dominate the LF at moderate luminosities $\sim L_*$ (the 'knee'). Merger-induced bursts increasingly dominate at $L \gg L_*$; at the most extreme luminosities, AGN are important. However, all populations increase in luminosity at higher redshifts, owing to increasing gas fractions. Thus, the 'transition luminosity' between normal and merger-dominated sources increases from the luminous infrared galaxy (LIRG)–ultraluminous infrared galaxy threshold at $z \sim 0$ to bright Hyper-LIRG thresholds at $z \sim 2$. The transition to dominance by obscured AGN evolves similarly, at factor of several higher $L_{\rm IR}$. At all redshifts, non-merging systems dominate the total luminosity/SFR density, with merger-induced bursts constituting ∼5–10 per cent and AGN ∼1–5 per cent. Bursts contribute little to scatter in the SFR–stellar mass relation. In fact, many systems identified as 'ongoing' mergers will be forming stars in their 'normal' (non-burst) mode. Counting this as 'merger-induced' star formation leads to a stronger apparent redshift evolution in the contribution of mergers to the SFR density. We quantify how the evolution in LFs depends on evolution in galaxy gas fractions, merger rates, and possible evolution in the Schmidt–Kennicutt relation. We discuss areas where more detailed study, with full radiative transfer treatment of complex three-dimensional clumpy geometries in mixed AGN–star-forming systems, is necessary.

Key words: galaxies: active – galaxies: evolution – galaxies: formation – cosmology: theory.

1 INTRODUCTION

Understanding the global star formation history of the Universe remains an important unresolved goal in cosmology. In recent years, observations of the properties of galaxies in the infrared (IR), at redshifts $z = 0$–3, have begun to shed light on this history, but have also revealed a number of intriguing questions.

Of particular interest are the roles of mergers and active galactic nuclei (AGN) in driving star formation and/or the IR luminosities of massive systems. A wide range of observed phenomena support the view that gas-rich[1] mergers are important to galaxy evolution; but, it is less clear what their role is in the global star formation process and buildup of stellar mass in the Universe. In the local Universe, the population of star-forming galaxies appears to transition from

⋆E-mail: phopkins@astro.berkeley.edu
†Hubble Fellow.

[1]By 'gas,' we refer specifically to cold, star-forming gas in galaxy discs, as opposed to hot, virialized gas.

'quiescent' (non-disturbed)[2] discs – which dominate the *total* star formation rate (SFR)/IR luminosity density – at the luminous infrared galaxy (LIRG) threshold $10^{11}\,L_{\odot}(\dot{M}_{*}\sim 10$–$20\,M_{\odot}\,yr^{-1})$ to clearly merging, violently disturbed systems at a few times this luminosity. The most intense starbursts at $z=0$, ultraluminous infrared galaxies (ULIRGs; $L_{IR}>10^{12}\,L_{\odot}$), are invariably associated with mergers (e.g. Joseph & Wright 1985; Sanders & Mirabel 1996; Evans et al. 2009), with dense gas in their centres providing material to feed black hole (BH) growth and to boost the concentration and central phase-space density of merging spirals to match those of ellipticals (Hernquist, Spergel & Heyl 1993; Robertson et al. 2006). Various studies have shown that the mass involved in these starburst events is critical to explain the relations between spirals, mergers and ellipticals, and has a dramatic impact on the properties of merger remnants (e.g. Lake & Dressler 1986; Doyon et al. 1994; Shier & Fischer 1998; James et al. 1999; Genzel et al. 2001; Tacconi et al. 2002; Dasyra et al. 2006, 2007; Rothberg & Joseph 2004, 2006; Hopkins et al. 2009a,e).

At high redshifts, the role of mergers is less clear. It is clear that LIRGs and ULIRGs increase in relative importance with redshift, with LIRGs dominating the SFR/IR luminosity densities at $z\sim 1$ and ULIRGs dominating at $z\sim 2$ (e.g. Le Floc'h et al. 2005; Pérez-González et al. 2005; Caputi et al. 2007; Magnelli et al. 2009). This, together with the fact that merger rates are expected and observed to increase with redshift (by a factor of $\sim$10 from $z=0$ to 2; see e.g. Hopkins et al. 2009g, and references therein), has led to speculation that the merger rate evolution may in fact drive the observed evolution in the cosmic SFR density, which rises rapidly from $z\sim 0$ to 2 and then turns over, declining more slowly (e.g. Hopkins & Beacom 2006, and references therein).

However, many LIRGs at $z\sim 1$, and potentially ULIRGs at $z\sim 2$, appear to be 'normal' galaxies, without dramatic morphological disturbances associated with the local starburst population or large apparent AGN contributions (Sajina et al. 2007; Yan et al. 2007; Dasyra et al. 2008; Dey et al. 2008; Melbourne et al. 2008). At the same time, even more luminous systems appear, including large populations of Hyper-LIRG (HyLIRG; $L_{IR}>10^{13}\,L_{\odot}$) and bright submillimetre galaxies (e.g. Chapman et al. 2005; Younger et al. 2007, 2009c; Casey et al. 2009). These systems exhibit many of the traits more commonly associated with merger-driven starbursts, including morphological disturbances, and may be linked to the emergence of massive, quenched (non star-forming), compact ellipticals at times as early as $z\sim 2$–4 (Papovich et al. 2005; Tacconi et al. 2006, 2008; Schinnerer et al. 2008; Younger et al. 2008b; Chapman et al. 2009). But, reproducing their abundance and luminosities remains a challenge for current models of galaxy formation (Baugh et al. 2005; Swinbank et al. 2008; Narayanan et al. 2009b; Younger et al. 2009a).

In a related vein, observations of a tight correlation between the masses of supermassive BHs and their host spheroid properties (Magorrian et al. 1998; Ferrarese & Merritt 2000; Gebhardt et al. 2000; Novak, Faber & Dekel 2006; Hopkins et al. 2007b) suggest a tight coupling between BH growth and star formation, perhaps in particular to the mergers believed to drive the formation of the most massive bulges. Considering the energy output required to form the BH population (e.g. Soltan 1982), or the observed bolometric quasar energy density as a function of redshift (see Hopkins et al. 2007c, and references therein), it is clear that the *bolometric* output of quasars and AGN is at least roughly comparable to the total IR luminosity density of the Universe at most redshifts ($z\sim 1-3$) – although the measurements above suggest it is still a factor of $\sim$2–3 lower. Some recent observations have suggested that the population of very luminous, highly obscured (Compton-thick) quasars may be considerably larger than previous estimates, in which case the heavily obscured AGN population could represent a large fraction of the total IR luminosity density at high redshifts (Daddi et al. 2007; Hickox et al. 2007; Treister, Urry & Virani 2009). This would have dramatic implications not just for BH populations and, for example, the implied radiative efficiencies of BH accretion but also for the implied total SFR density. Some apparent discrepancies between, for example, the total mass density observed in old stars and the implied SFR density have been cited as possible evidence of a time-dependent stellar initial mass function (IMF); but, a rising contribution from obscured AGN at high redshifts could mimic this effect (Hopkins & Beacom 2006; Davé 2008).

In particular, there are long-standing questions of what powers the most luminous IR sources, for example, ULIRGs and submillimetre galaxies. This debate extends to the discovery of these objects (see e.g. Soifer et al. 1984, 1987; Scoville et al. 1986; Sargent et al. 1987; Sanders et al. 1988b; Solomon et al. 1997), and has persisted despite the addition of millimetre spectroscopy and observations in a large number of independent wavebands (for a review of the debate, see both Sanders 1999; Joseph 1999). Although some evidence suggests that they are primarily powered by star formation (Farrah et al. 2003; Lutz et al. 1998; Sajina et al. 2007; Pope et al. 2008a,b; Nardini et al. 2009; Watabe et al. 2009), the constraints and correlations typically invoked have inherent factor of $\sim$2 uncertainties, and thus could easily accommodate comparable power input from star formation and AGN. Moreover, a sufficiently obscured AGN, in a medium with the right optical depth properties, is indistinguishable from star formation by the usual indicators (e.g. polycyclic aromatic hydrocarbon (PAH) strengths, emission region sizes or any other IR spectral or morphological criteria). Hence even at $z=0$, debate surrounds the power source of many bright IR systems, and there exist a number of examples of systems classified as 'star formation dominated' by all of these metrics that later revealed Compton-thick AGN whose longer wavelength emission has been fully reprocessed, even into 'cool' dust (see e.g. Alexander et al. 2008, and references therein). In a bolometric sense, the most luminous galaxies observed (with $L\gtrsim 10^{14}\,L_{\odot}$ or $\gg 10^{47}\,erg\,s^{-1}$) are the most luminous quasars, although the contribution of these systems to the IR remains highly uncertain. This may be important for resolving the theoretical difficulties in modelling these bright systems.

There has been important theoretical progress in modelling these processes in an a priori manner (see e.g. Baugh et al. 2005; Hopkins et al. 2008d; Narayanan et al. 2009b; Younger et al. 2009a). However, two basic limitations remain. In direct cosmological hydrodynamic simulations, as well as semi-analytic models of galaxy formation, it is well known that it remains challenging to accurately reproduce global quantities such as the galaxy mass function (MF) and the distribution of sizes, gas fractions, and hence SFRs, especially the distributions of star-forming gas and their relations to whether or not galaxies are 'quenched' (recently, see e.g. Maller et al. 2006; Weinmann et al. 2006; Kimm et al. 2009; Fontanot et al. 2009). This makes it difficult to determine whether discrepancies between such models and the observations owe to their treatment of star formation, or to discrepancies in these

[2]In this paper, we use the term 'quiescent' to refer to star-forming systems that are not strongly disturbed in , for example, major mergers and are forming stars in similar fashion to most 'normal' discs. We do *not* mean non-star-forming systems, as the term is used in some literature.

quantities. Moreover, it is difficult to disentangle the effects of these different properties on the distribution of SFRs. In addition, for merger-induced starburst and AGN activity, although it may be possible to roughly estimate some global quantities (e.g. the total mass involved in a starburst) from simple analytic motivations or low-resolution cosmological simulations (several ∼kpc typical), it is not straightforward to estimate the chaotic, time-dependent behaviour of full light curves needed to estimate the distribution of time spent at different, rapidly varying luminosities without high-resolution simulations of individual systems. Since the number density of the most bright systems is exponentially declining, fluctuations and features in the starburst/AGN fuelling history on small time and spatial scales ($\Delta t \sim 10^7$ yr, $R \lesssim 100$ pc) can be critical for correct estimates of their contributions to bright populations.

In this paper, we present theoretical predictions for the distribution of galaxy SFRs and IR luminosities, as a function of galaxy mass and redshift, using a novel methodology that can circumvent some of these obstacles. We combine a halo-occupation based approach, in which we take galaxy properties as fixed from observations at each epoch, and then apply rules for the distribution of SFRs/IR luminosities in 'quiescent' systems, merger-induced starbursts and obscured AGN, calculated from a large suite of high-resolution hydrodynamic simulations of individual galaxies and galaxy mergers. We use this to independently estimate the contributions of 'normal' galaxies, mergers and AGN to the luminosity functions (LFs). The comparisons we make are approximate – we do not include full time-dependent radiative transfer in simulations (the subject of future work, in progress), and so focus on integral quantities such as the total IR luminosity and SFR distributions, that are less sensitive to issues of, for example, the exact dust distribution, temperature and other properties. We also explicitly separate the contributions of AGN and star formation, but stress that, in real systems where the two are comparable, their additive effects are non-linear and will require further study. We show how adding or removing components of the model taken from observations such as, for example, the distribution of galaxy sizes and gas fractions affects these consequences. We compare to observations of all quantities, where available, and find reasonable agreement but with some interesting apparent discrepancies at high redshifts. We also show how these populations relate to the scatter in SFRs at fixed galaxy masses, and in a global sense to the total SFR density, the SFR density in mergers and the fraction of the inferred SFR density which might really be driven by obscured AGN activity. Readers interested primarily in the comparison of predictions and observations may wish to skip directly to Section 3.

Throughout, we adopt a $\Omega_{\rm M} = 0.3, \Omega_{\Lambda} = 0.7, h = 0.7$ cosmology and a Chabrier (2003) stellar IMF (discussed further below), but these choices do not affect our conclusions.

2 THE MODEL

The model used here is a slightly modified version of one that has been discussed extensively in a series of papers (most recently Hopkins et al. 2009f,g). We summarize the salient properties here. Fig. 1 provides a simple outline of the model, on which we elaborate below.

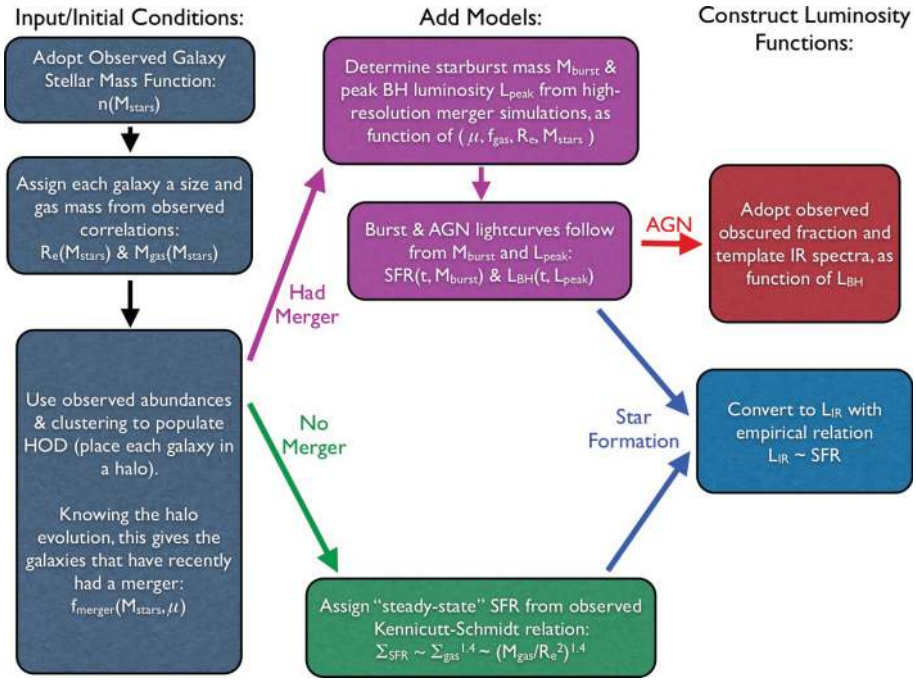

Figure 1. Summary of our model methodology, described in detail in Section 2. We begin with a halo occupation model: at a given redshift, the galaxy stellar MF and distribution of galaxy sizes and gas fractions are taken from observations. Placing galaxies in haloes from dark matter simulations according to their observed abundance and clustering, and evolving these forward in time some short time, we obtain the merger population. Non-merging galaxies are assigned a SFR based on their size and gas mass, according to the observed Kennicutt–Schmidt relation; for mergers, the light curves of merger-induced starburst and AGN activity are taken from fits to high-resolution galaxy merger simulations (including star formation based on a local Kennicutt–Schmidt law, gas cooling and feedback from accretion and star formation), as a function of salient galaxy properties. Star formation rates are converted to IR luminosities with a simple empirical proportionality; AGN bolometric luminosities are corrected to far-IR luminosities based on observed obscured fractions.

2.1 Halo occupation constraints: the initial galaxy population from observations

At a given redshift, we use the halo occupation distribution (HOD) formalism to construct a mock sample of galaxies. Specifically, we begin with the observed galaxy stellar MF, which we take as given. Since we are interested specifically in star-forming galaxies, we adopt just the galaxy stellar MF of star-forming or 'blue' galaxies where available (here at all $z < 2$); although there may be some trace star formation in red galaxies, assuming typical values yield a negligible contribution to the bright far-IR and massively star-forming populations. At redshifts $z > 2$, type-separated MFs are no longer available, so we simply adopt the total galaxy MF (i.e. assume all systems are star forming); however, the fraction of massive galaxies that are 'quenched' and red has become sufficiently low by $z = 2$ (and is rapidly falling) that it makes little difference (e.g. adopting the upper limit – that the red fraction at all masses at $z > 2$ is equal to that at $z = 2$ – makes no difference to our predictions).

The uncertainties in the galaxy abundance are one of the dominant uncertainties in the model, especially at high redshifts. We therefore consider different MF fits, to represent the possible range. At $z = 0$, the uncertainties are relatively small; we adopt the MF of star-forming galaxies from Bell et al. (2003). From $z = 0$–2, we consider the MFs of star-forming galaxies from Arnouts et al. (2007) and Ilbert et al. (2009). The range between the two is representative of the uncertainties and scatter in a number of other calculations, which cover different portions of this dynamic range (e.g. Bundy, Ellis & Conselice 2005; Borch et al. 2006; Fontana et al. 2006; Franceschini et al. 2006; Pannella et al. 2006; Brown et al. 2007). At $z > 2$, we adopt as bracketing the relevant dynamic range the MFs from Pérez-González et al. (2008) and Fontana et al. (2006); again, other determinations (e.g. Kajisawa et al. 2009; Marchesini et al. 2009) lie within this range.

Given each galaxy and its stellar mass, we assign it other properties in accord with observations. First, a gas mass. It is well established that, at fixed stellar mass, galaxy gas fractions are higher at high redshifts (see compiled references below). Moreover, the trend of galaxy gas fractions as a function of stellar mass, and their scatter, has been quantified (both directly and indirectly) at a range of redshifts from $z = 0$ to 3. We have compiled observations from the available sources, spanning this redshift range and a stellar mass range from $M_* \sim 10^{10}$ to $10^{12}\,\mathrm{M}_\odot$ (more than sufficient dynamic range for the predictions of interest here), specifically from Bell & de Jong (2000), McGaugh (2005), Calura et al. (2008), Shapley et al. (2005), Erb et al. (2006), Puech et al. (2008), Mannucci et al. (2009), Cresci et al. (2009), Förster Schreiber et al. (2009) and Erb (2008). We present these observations in a number of papers (Hopkins et al. 2007a, 2008b,d) and show that the $z = 0$ zero-point and evolution with redshift can be well-fitted by the simple functions

$$f_{\rm gas}(M_*|z=0) \equiv f_0 \approx \frac{1}{1+(M_*/10^{9.15})^{0.4}},$$
$$f_{\rm gas}(M_*|z) \quad = f_0\,[1-\tau(z)\,(1-f_0^{3/2})]^{-2/3}\,, \tag{1}$$

where $\tau(z)$ is the fractional look back time to a redshift z ($\equiv 0$ at $z = 0$ and $\equiv 1$ at $z \rightarrow \infty$). The former functional form is motivated by cosmological hydrodynamic simulations (Kereš et al. 2005, 2009), and the latter by the scalings of simple closed box models that obey the Kennicutt (1998) relation at all times.[3] The important quantity is not the precise scaling but rather the fact that it provides a convenient interpolation formula between the observations above. We assume a constant, intrinsic 0.25 dex scatter about these gas masses at each stellar mass, also in agreement with the observations above.

Next, we assign galaxy spatial sizes, again from observations. At $z = 0$, the distributions of disc sizes are well measured; at higher redshifts, there is some uncertainty, but observations are converging on the conclusion that the star-forming population evolves relatively mildly in size with redshift (whereas the non-star-forming population evolves more rapidly). From $z = 0$ to 2, we find that the compilation of observational results on the evolution of the disc size–mass relation from Trujillo et al. (2004), Ravindranath et al. (2004), Ferguson et al. (2004), Barden et al. (2005), Toft et al. (2007), Akiyama et al. (2008), and the theoretical models in Somerville et al. (2008), can be simply represented as relatively weak power-law evolution in disc size at fixed mass,

$$R_e(M_*|z=0) \approx 5.28\,\mathrm{kpc}\left(\frac{M_*}{10^{10}\,\mathrm{M}_\odot}\right)^{0.25},$$
$$R_e(M_*|z) = R_e(M_*|z=0)\,(1+z)^{-0.6}, \tag{2}$$

where the $z = 0$ relation is taken from Shen et al. (2003) (appropriately normalized for our adopted cosmology and IMF), and we assume a constant 0.2 dex scatter in disc sizes. As we will show, our results are not especially sensitive to the adopted size evolution, so this is not a major source of uncertainty.

2.2 'Normal' star formation: relation to galaxy properties

Our major assumption is the Kennicutt–Schmidt law holds at all redshifts, relating the (average) surface density of star formation to the average surface gas density

$$\dot{\Sigma}_* = 1.3\times10^{-4}\,\mathrm{M}_\odot\,\mathrm{yr}^{-1}\,\mathrm{kpc}^{-2}\left(\frac{\Sigma_{\rm gas}}{\mathrm{M}_\odot\,\mathrm{pc}^{-2}}\right)^{n_K} \tag{3}$$

with the best-fitting index $n_K \approx 1.4$ (Kennicutt 1998). The normalization here is corrected for our assumed Chabrier (2003) IMF. We will later consider the index and normalization to be free, but for now take this relation as fixed. Some simple algebra shows that this (assuming no dramatic evolution in disc profile shapes) can be written in the global form

$$\frac{\dot{M}_*}{\mathrm{M}_\odot\,\mathrm{yr}^{-1}} = 1.3\left(\frac{10^4}{\pi}\right)^{n_K-1}\left(\frac{M_{\rm gas}}{10^{10}\,\mathrm{M}_\odot}\right)^{n_K}\left(\frac{R_e}{\mathrm{kpc}}\right)^{-2(n_K-1)}. \tag{4}$$

Together with the assumptions above, this defines a 'steady-state' or 'quiescent' SFR for all discs in the model.

We will show that the resulting SFR distributions agree well with those observed for normal galaxies, suggesting that these scalings are reasonable. However, we have also checked them against direct observations of the median SFR of disc galaxies as a function of stellar mass and redshift. These are measured in Noeske et al. (2007a) from $z = 0$ to 1.2 and in Papovich et al. (2006) at $z \sim 2$;

[3] This function is presented in Hopkins et al. (2009c), equation (2); we note that in the text there is a typo, and the equation is written with a $+\tau(z)$. The correct form (above) with $-\tau(z)$ was, however, used for the calculations therein.

comparing with the simple predictions from equation (4) and the equations above yields reasonably good agreement. The combined dependence of $f_{\rm gas}(M_*)$ and $R_e(M_*)$ means that $\dot{M}_*(M_*)$ weakly increases with M_* in a roughly power-law like fashion, in good agreement with these observations; and the redshift dependence of $f_{\rm gas}$ yields a similar increase in the normalization of the SFRs with redshift (and by construction, the $z = 0$ normalizations are similar). In fact, we find that our results for the quiescent disc population are completely unchanged (within their uncertainties) if we simply adopt a parametrized fit to the observations in these papers – i.e. if we bypass all of the above assumptions and simply adopt a fit to the observed $\dot{M}_*(M_*|z)$ relations. However, this would severely limit the dynamic range in redshift and mass to which we could robustly apply these models, as well as limiting the physical insight gained, and (most of all) would not allow for the straightforward predictions for merger and AGN populations.

2.3 Merger rates and resulting starburst properties

We next require a model for merger rates, in order to model merger-induced bursts of star formation and AGN activity. The methodology for doing so is described and tested in Hopkins et al. (2009g), but we briefly summarize here.[4] We assign each galaxy to a halo or subhalo in a simple manner following the standard halo occupation methodology described in Conroy & Wechsler (2009); ensuring, by construction, that the galaxy MF and galaxy clustering (as a function of stellar mass, galaxy colour and physical scale) are exactly reproduced. At a given instant, then knowing the halo–halo merger rates as a function of, for example, halo mass and mass ratio, we can convolve this with the determined galaxy masses in each halo (and appropriately correct for, for example, the dynamical friction time delay between halo–halo and galaxy–galaxy merger, following Boylan-Kolchin, Ma & Quataert 2008), and obtain the galaxy–galaxy merger rate as a function of galaxy mass M_*, redshift z and galaxy–galaxy baryonic (or stellar) mass ratio $\mu \equiv M_2/M_1$ (defined always so that $M_1 > M_2$, i.e. $0 < \mu < 1$). The halo MFs and merger rates are adopted from the Millenium Simulation (Springel et al. 2005b; Fakhouri & Ma 2008); but, in Hopkins et al. (2009g) we compare this with a wide variety of alternative simulations and calculations, as well as a number of differences in methodology, and show that these all lead to small (a factor of <2) differences in the resulting merger rate. In that paper, we also compare this calculation to a large number of observational constraints in the redshift range $z = 0 - 2$ (see references therein), and show that the two agree well; adopting a parametrized fit to the observed major merger rate from most observations yields an identical result in our calculation here (but does not have the convenience of being easy to extrapolate to arbitrary mass ratios μ or redshifts z). Note that, again, we begin from just the star-forming galaxy LF – 'dry' mergers of quiescent systems will not produce interesting starburst or AGN activity.

In a merger, gravitational torques lead to gas in the disc rapidly losing angular momentum to the nearby stars, and falling inwards (Barnes & Hernquist 1991, 1996). The rapid increase in the central gas densities drives a massive starburst (Mihos & Hernquist 1994, 996). Here, we assume that every merger induces a starburst and corresponding AGN activity. In Hopkins et al. (2009b), as well as a number of other studies (see e.g. di Matteo et al. 2007; Cox et al. 2008; Hopkins et al., in preparation, and references therein), the resulting total starburst mass/amplitude and peak quasi-stellar object (QSO) luminosity are quantified as a function of merger properties, from a suite of hundreds of high-resolution hydrodynamic galaxy merger simulations. These simulations span a range in the relevant properties: redshift; merger mass ratio; orbital parameters; galaxy structural properties and gas fractions, and they include prescriptions based on the same Kennicutt (1998) law for dynamic star formation, as well as BH accretion and feedback from supernovae and AGN (Di Matteo, Springel & Hernquist 2005; Springel, Di Matteo & Hernquist 2005a). Together this allows for a full sampling of the interesting parameter space and a simple, direct parameterization of the resulting burst properties.

Despite the complex physics involved, it is shown therein that the average burst scalings can be represented in analytic form, motivated by basic gravitational physics. We adopt the full scalings derived therein, but note that the important parameter, the *total* mass of gas that loses angular momentum and participates in the central starburst, scales (to lowest order) with the simple relation (after averaging over a random distribution of orbital parameters)

$$M_{\rm burst} \sim M_{\rm gas}\,\mu\,(1 - f_{\rm gas}). \tag{5}$$

The scaling with merger mass ratio μ represents the declining efficiency of angular momentum loss in more minor mergers; the scaling with $(1 - f_{\rm gas})$ comes from the fact that the torques that remove angular momentum from gas are primarily *internal*, from stars in the same galaxy – a pure gas merger would simply yield a new disc, not a compact starburst.[5] Adopting the simplified scaling above, in fact, yields very similar results to the full scaling presented in Hopkins et al. (2009b) for $M_{\rm burst}$ as a function of μ, $M_{\rm gas}$, $f_{\rm gas}$ and orbital parameters (we assume random orbital inclinations and parabolic orbits, motivated by cosmological simulations). Motivated by the simulations (or e.g. allowing for the full distribution of orbital parameters), we adopt a constant 0.35 dex scatter in $M_{\rm burst}$ at fixed galaxy properties (with of course the limit $M_{\rm burst} < M_{\rm gas}$).

In a burst, there is some non-trivial time-dependent light curve or SFR versus time. Since we are considering the statistical distribution of luminosities, we do not need to know the exact time-dependent form of this function; rather, the important quantity is the distribution of times spent at different luminosities. Examples of this are shown in detail in Hopkins et al. (2006c), and similar quantities are presented in di Matteo et al. (2007) and Cox et al. (2008). We find that, integrated over the history of a burst, this function can (on average) be conveniently represented by the simple function:

$$\frac{{\rm d}t}{{\rm d}\log \dot{M}_*} = t_{\rm burst}\,\ln 10\,\exp\left(-\frac{\dot{M}_*}{M_{\rm burst}/t_{\rm burst}}\right), \tag{6}$$

[4]The approximate merger rates from the model presented in Hopkins et al. (2009g) can also be obtained as a function of galaxy mass, merger mass ratio, and gas fraction from the publicly available 'merger rate calculator' script at http://www.cfa.harvard.edu/phopkins/Site/mergercalc.html.

[5]The physics of these scalings, particularly that with gas fraction, is discussed in detail in Hopkins et al. (2009b). In short, hydrodynamic torques and pressure forces are negligible, and direct torques from, for example, the secondary galaxy and halo are suppressed by a tidal term $\sim(r/R_e)^3$, the short time of close passage (much less than the several dynamical times needed to continue strong gas inflows) and the fact that they are out of resonance with the primary gas disc. Moreover these torques are just as likely to increase as decrease the gas angular momentum. As shown in that paper and earlier (Barnes & Hernquist 1996; Barnes 1998), this means that the stellar disc in the same galaxy [with fractional mass $(1 - f_{\rm gas})$], being in direct spatial proximity and resonance, always dominates the torques driving angular momentum loss in the gas.

where, fitting to the simulations, we find $t_{\rm burst} \approx 0.1$ Gyr, nearly independent of galaxy mass and redshift. This functional form is characteristic of a rapid, exponential rise from low SFR to a peak in the burst, with a burst lifetime of the order of $t_{\rm burst}$. The constancy and normalization of this lifetime is a simple consequence of the observed dynamical times in the central regions of galaxies, and the fact that these dynamical times scale weakly or not at all with mass and redshift (see e.g. Bell & de Jong 2001; McGaugh 2005; Courteau et al. 2007). Given some merger rate, and corresponding rate of 'creation' of bursts of a given mass $[{\rm d}n(M_{\rm burst})/{\rm d}t]$, the observed number density of bursts at a given $\dot{M}_*$ is simply given by the convolution of this rate with the lifetime above, i.e. ${\rm d}n(M_{\rm burst})/{\rm d}\log\dot{M}_* = [{\rm d}n(M_{\rm burst})/{\rm d}t]({\rm d}t/{\rm d}\log\dot{M}_*)$ (for more explicit details of this methodology, see Hopkins et al. 2006a).

Note that the numbers above are somewhat different from those presented in Hopkins et al. (2006c). However, in that paper, we were considering the total distribution of SFRs that would be observed over the *entire* duration in which a system might be identified as a merger or interacting pair. The lifetime of that phase is much longer, ∼1–2 Gyr, and (by time and by total mass) most of the star formation comes from the 'normal' star formation that would be associated with the two merging discs independently (see e.g. di Matteo et al. 2007; Cox et al. 2008). Depending on the observational criteria used to identify mergers, of course, this definition of star formation 'in mergers' may be of interest. It is, however, a subset of the 'quiescent' star formation for the most part, and is distinct physically (and very distinct in terms of the imprint that it leaves on galaxy stellar populations, kinematics and structural properties) from the short-lived, compact burst specifically *induced* by the merger.

2.4 AGN and quasars

Given some merger, quasar activity is also excited; to lowest order in simulations with AGN feedback, the peak bolometric luminosity of the AGN is tightly coupled to the total bulge mass that will be formed from a disc–disc merger. The total bulge mass is the burst mass (discussed above), plus the violently relaxed stellar disc mass, which is simply $M_{\rm relaxed} \approx \mu\, M_*$ in simulations and from simple gravitational physics considerations (again, see Hopkins et al. 2009b). At fixed bulge mass, the peak AGN luminosity, corresponding to the Eddington limit of the maximum BH mass, is coupled to this bulge mass as it must overcome its binding energy in order to halt continued growth. In Hopkins et al. (2007a,b), we show how this scales in simulations with bulge mass and other properties. We find that it can be conveniently represented by the scaling

$$L_{\rm peak,\,QSO} \approx 4.6\times10^{11}\,{\rm L}_\odot \times (1+z)^{0.5}\left(\frac{M_{\rm burst}+M_{\rm relaxed}}{10^{10}\,{\rm M}_\odot}\right). \quad (7)$$

The latter scaling simply reflects the fact that the peak/final BH mass scales roughly linearly with total bulge mass, in both observations and simulations. The $(1+z)^{0.5}$ scaling comes from the simulations discussed in Hopkins et al. (2007a); it comes from the fact that galaxies at high redshift, being both more gas-rich and more compact, require more 'work' to be done by the AGN before it can self-regulate its luminosity/BH mass, and so yield higher BH masses at otherwise fixed bulge mass. We refer to that paper for more details, but note that the other parameterizations of this evolution (discussed therein) yield nearly identical results. Likewise, other models for AGN self-regulation at high masses and/or luminosities predict a similar maximum BH mass as a function of host galaxy properties (Silk & Rees 1998; Murray, Quataert & Thompson 2005; Shankar 2009), and the resulting 'cut-off' in the AGN luminosities at high masses (owing to self-regulation combined with a cut-off in the depth of host galaxy potential wells) is similarly predicted in, for example, Natarajan & Treister (2009). Moreover, such moderate evolution in $M_{\rm BH}/M_*$ is suggested by a number of observations (e.g. Peng et al. 2006; Woo et al. 2006; Salviander et al. 2007; Treu et al. 2007, and references therein). Motivated by the simulations and the observed BH-host correlations, we assume a constant 0.3 dex scatter in these relationships.

In what follows, we consider only AGN induced in mergers, but stress that this does include non-trivial contributions from minor mergers down to, for example, mass ratios of ∼1:10. There is considerable debate regarding whether or not entirely non-merger processes such as stellar bars (e.g. Shlosman, Frank & Begelman 1989; Jogee 2006; Younger et al. 2008a, and references therein) and/or stochastic encounters with molecular clouds (Hopkins & Hernquist 2006; Nayakshin & King 2007) might drive significant AGN activity. However, it is generally clear both from observations and from simple theoretical considerations that the resulting AGN would be important only at low luminosities. Hopkins & Hernquist (2009a) compile both empirical and theoretical estimates of the luminosities below which non-merger processes dominate AGN fuelling and find consistently that this is exclusively in the traditional Seyfert regime ($L_{\rm bol} \lesssim 10^{12}\,{\rm L}_\odot$; see Malkan, Gorjian & Tam 1998; Canalizo & Stockton 2001; Dunlop et al. 2003; Kauffmann et al. 2003; Floyd et al. 2004; Guyon, Sanders & Stockton 2006; Hutchings et al. 2006; Zakamska et al. 2006; Rigby et al. 2006; Urrutia, Lacy & Becker 2008; Zakamska et al. 2008). This is clear from integral constraints; bulges formed in bars ('pseudo-bulges') or non-merging bulges with bars or central molecular gas concentrations dominate only at low galaxy masses, in galaxy types of Sb/c and later (Kormendy & Kennicutt 2004; Allen et al. 2006; Fisher 2006; Driver et al. 2007; Fisher & Drory 2008). Given the observed BH-host correlations, this corresponds to BHs with masses $\lesssim 10^7\,{\rm M}_\odot$, or maximum luminosities at the Eddington limit of $L_{\rm bol} = 3\times10^{11}\,{\rm L}_\odot$. But, as we will show AGN are significant in the IR LF only at the highest luminosities, $L > 10^{13}\,{\rm L}_\odot$ – i.e. BHs with $\sim10^9\,{\rm M}_\odot$ at Eddington, with accretion rates of $>10\,{\rm M}_\odot\,{\rm yr}^{-1}$. Since it is unlikely that these extreme systems are powered in non-violent events, our neglect of non-merger induced AGN makes little difference to our predictions. We have, in fact, explicitly checked whether including them (according to the model LFs predicted in Hopkins & Hernquist 2006) makes any difference, and find it only increases the very low-luminosity contributions of AGN by a factor of ∼2–3, far less than the approximately three to four orders of magnitude required to substantially change our conclusions. Likewise, simply adopting the observed AGN bolometric LFs – including all observed AGN – from Hopkins et al. (2007c) or Shankar, Weinberg & Miralda-Escudé (2009) with our estimated template spectra and obscured fractions, we find no significant difference.

For a given peak BH mass or peak luminosity, we simply require again the distribution of luminosities corresponding to the average light curve, in order to construct the number density as a function of luminosity. These light curves and the resulting distribution of time spent at different AGN luminosities (both bolometric and in various observed bands) have been extensively discussed in a series of papers (Hopkins et al. 2005a,b,d, 2006a,b). We adopt the

Schechter-function parameterization therein,

$$\frac{\mathrm{d}t}{\mathrm{d}\log L_{\rm bol}} \approx 0.22\,\mathrm{Gyr}\left(\frac{L_{\rm bol}}{L_{\rm peak}}\right)^{\alpha}\exp\left[-\left(\frac{L_{\rm bol}}{L_{\rm peak}}\right)\right],$$
$$\alpha \approx -0.44 + 0.21\,\log\left(L_{\rm peak}/10^{12}\,\mathrm{L}_{\odot}\right), \quad (8)$$

Again, this is taken from simulations, but in those papers it is shown that this yields very good agreement with the observed distribution of AGN Eddington ratios, host masses and luminosities, and the evolution of the AGN LF (most recently, see Volonteri, Salvaterra & Haardt 2006; Hopkins et al. 2008d; Bonoli et al. 2009; Foreman, Volonteri & Dotti 2009; Hopkins & Hernquist 2009a,b; Marulli et al. 2009).

2.5 Construction of IR luminosity functions

Finally, given these predicted SFR and AGN bolometric luminosity distributions, we need to convert to the observable quantity, namely total IR luminosity. Because we are not attempting to model the full spectral energy distributions (SEDs) and dust physics of these systems, the only quantity that we can robustly predict is the *total* IR luminosity, $L_{\rm IR}$, defined as the integrated luminosity from 8 to 1000 μm. In the case of SFR distributions, we adopt the simple conversion from Kennicutt (1998), corrected for our adopted Chabrier (2003) IMF, of

$$L_{\rm IR} = 1.1\times10^{10}\,\mathrm{L}_{\odot}\left(\frac{\dot{M}_{*}}{\mathrm{M}_{\odot}\,\mathrm{yr}^{-1}}\right). \quad (9)$$

Note that more sophisticated (e.g. luminosity-dependent) conversions have been proposed, but since this choice is used to calibrate the gas surface density–SFR surface density relation we adopt it for consistency. In any case, alternative formulations largely deviate from the above only in non-starburst or lower IR-luminosity galaxies, where absorption is weaker, but these are not particularly important for our comparisons here, and experimenting with those in Buat & Burgarella (1998) and Jonsson et al. (2006) yields almost no difference at $L_{\rm IR} > 10^{11}\,\mathrm{L}_{\odot}$.

An advantage of our semi-empirical model is that our conclusions do not depend significantly on the adopted stellar IMF, for typical choices. Altering the IMF between, for example, Chabrier (2003), Kroupa (2002), Scalo (1986) or, for example, Salpeter (1955) generally amounts to systematic changes in the mass-to-light ratio M_{*}/L by up to 0.3 dex. However, because we begin with observed galaxy properties and calculate observed LFs, this systematic dependence cancels out. Specifically, in adopting the observed Kennicutt (1998) relation, the observable quantity is the luminosity surface density – this factor enters in the conversion to a SFR surface density. But then, converting the resulting SFR to an observed luminosity, the same factor enters, cancelling out. Explicitly recalculating our predictions with other IMF choices confirms this. The only residual effects are second order, and relatively weak – for example, changing the implied gas exhaustion time-scale leads to slightly different dynamics of the gas on small scales in mergers. Such details are outside the scope of our comparison here, and in any case amount to smaller effects than our systematic uncertainties. In an a priori model for star formation, on the other hand, the factor would enter fully. The IMF will only present a systematic source of uncertainty in our predictions if it evolves significantly with redshift or galaxy properties, or if it is extremely top-heavy, possibilities we discuss further below.

For AGN, the conversion from bolometric to IR luminosities is somewhat more complex – unobscured (type 1) AGN reradiate only a fraction of ∼1/40−1/20 of their bolometric luminosity in the FIR, and are thus negligible for the LFs here. We adopt the empirically calculated obscured fraction as a function of quasar luminosity from Gilli, Comastri & Hasinger (2007), and assume that the obscured bolometric luminosity is reradiated in the IR; this allows us to convert our predicted bolometric quasar luminosity function (QLF) to an IR QLF of obscured quasars. Technically, not all of the luminosity will be obscured, of course, but we find that, for example, using the full distribution of column densities as a function of quasar luminosity from Ueda et al. (2003) to attenuate a template AGN SED yields a very similar answer (see also Franceschini et al. 2005), as does using a mean X-ray to IR bolometric correction of obscured AGN (Elvis et al. 1994; Zakamska et al. 2004; Polletta et al. 2006). The obscured AGN fraction at high luminosities remains uncertain; Hasinger (2008) argue that it could be lower by a factor of several than the Gilli et al. (2007) estimate at the highest luminosities (although this is redshift dependent and at $z \geq 1.5$ the two estimates agree well), whereas Daddi et al. (2007) argue that the number of obscured quasars should be a factor of ∼2–3 higher. These uncertainties are generally comparable to (or up to factor ∼2 larger than) the uncertainties from the choice of stellar MF, and we discuss some implications below.

3 STAR FORMATION RATE DISTRIBUTIONS AND INFRARED LUMINOSITY FUNCTIONS

3.1 Basic predictions

Fig. 2 shows the resulting predicted total-IR LFs from $z = 0$ to 6, divided into the contributions from 'normal' (non-merging, quasi-steady-state) star-forming systems, merger-induced 'bursts' and obscured AGN. As discussed in Section 2, we have recalculated our model adopting at least two different stellar MF determinations at each redshift; the range between the two at each redshift is shown

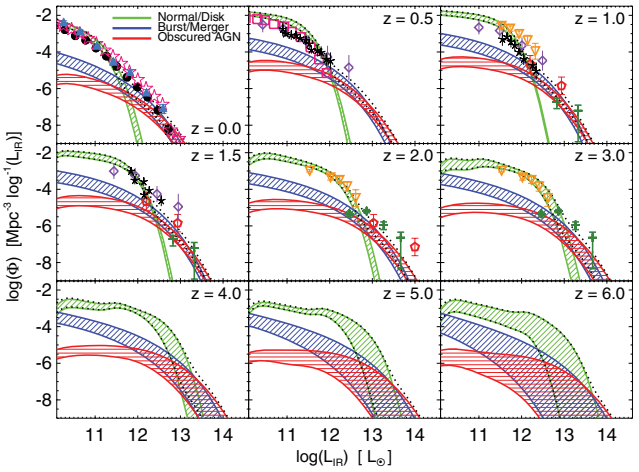

Figure 2. Total (8−1000 μm) IR LFs as a function of redshift. We show the model contribution from 'normal' (non-merging) star-forming discs (green), merger-induced starbursts (blue) and obscured AGN (red). The range in the total (summed) LF is shown with dotted black lines. Shaded ranges reflect the uncertainty from different stellar MF observations used in constructing the model. Points show observational estimates from Saunders et al. (1990, magenta stars), Soifer & Neugebauer (1991, blue triangles), Yun, Reddy & Condon (2001, black circles), Huang et al. (2007, magenta squares), Le Floc'h et al. (2005, violet diamonds), Caputi et al. (2007, orange inverted triangles), Magnelli et al. (2009, black ∗), Babbedge et al. (2006, red pentagons), Chapman et al. (2005, dark green +).

by the shaded range, and is representative of the scatter in different observational estimates. Unsurprisingly, this uncertainty is substantial at high redshifts. We also add (in quadrature) a systematic factor of ∼2 uncertainty in galaxy–galaxy merger rates, representative of the systematic theoretical and observational uncertainties as estimated from the compilations in Hopkins et al. (2009g). We add a factor 1.5 additional uncertainty in the AGN obscured fractions, again representative of systematic observational uncertainties (see e.g. Hopkins et al. 2005c, 2009d, Shi et al. (2006), Treister & Urry (2006), Hasinger (2008), and references therein). We also note that direct observational constraints used for our models of the galaxy stellar MF are either non-existent or extremely uncertain above $z > 4$; we extrapolate the fitted LF parameters from $z = 2$ to 4 into this redshift range, and so the resulting predictions should be treated with the appropriate caution.

We compare with observations of the IR LFs where available, from $z = 0$ to 3. Note that all of these are corrected to a total IR luminosity from observations in some band; we adopt the corrections compiled in Valiante et al. (2009), but emphasize that some caution, and at least a systematic factor of ∼2 uncertainty in $L_{\rm IR}$, should be considered in estimates from most if not all observed wavelengths. The agreement between the total predicted LF and the observations is generally reasonable, at most redshifts. At the highest luminosities and redshifts, specifically the submillimetre population observed in Chapman et al. (2005), we appear to underpredict the abundance of bright systems, but these observations are very uncertain. Austermann et al. (2010), for example, find that the millimetre number counts in these surveys are strongly affected by cosmic variance, and may be factors of several larger than the cosmic mean. We discuss this in Section 4, but note for now that these systems contribute relatively little to the global SFR density at these redshifts.

At all redshifts, 'quiescent' galaxies dominate the LF at low luminosities and high space densities, reflecting the abundance of star-forming discs and relative rarity of mergers and quasars. At higher luminosities, eventually merger-induced star formation and AGN activity become dominant, as expected in order to explain the most extreme (but short-lived) bursts of star formation. However, both types of systems increase in luminosity with redshift from $z =$ 0–3 in similar fashion.

As discussed in Section 2.5, the obscured AGN fraction is somewhat uncertain. However, Fig. 2 shows that even at extreme luminosities the contribution from obscured AGN is comparable to that from merger-induced starbursts. Thus, in terms of the total IR LF, even an obscured AGN fraction of zero would only lead to factor of ∼2 changes in the predicted bright-end number densities (smaller than the uncertainties owing to the choice of MF, for example).

To facilitate future comparisons with observations, we present the corresponding predictions in Appendix A for the IR LF in various specific rest-frame wavelengths. However, we stress that these are *not* direct predictions of the model – a proper model for the SEDs will depend on full radiative transfer models, applied to the simulations as a function of time and galaxy properties (these will be presented in a future work). Here, we simply convert total IR luminosities to wavelength-dependent luminosities using the same bolometric corrections used to convert the observations in Fig. 2.

3.2 Fitting functions to the predicted LFs

For the sake of comparison with future observations, we provide fits to the model predictions in Table 1. We find that the predicted IR LFs for each type can be reasonably represented by a double power-law model, i.e.

$$\Phi \equiv \frac{{\rm d}n}{{\rm d}\log L} = \frac{\phi_*}{(L/L_*)^{\alpha} + (L/L_*)^{\beta}}, \tag{10}$$

where the parameters ϕ_* (normalization), L_* (break luminosity), α (faint-end slope, i.e. $\Phi \propto L^{-\alpha}$ for $L \ll L_*$) and β (bright-end slope, i.e. $\Phi \propto L^{-\beta}$ for $L \gg L_*$) depend on redshift, with that dependence conveniently approximated as

$$\begin{aligned} \log L_* &= L_0 + L'\,\xi + L''\,\xi^2, \\ \log \phi_* &= \phi_0 + \phi'\,\xi + \phi''\,\xi^2, \\ \alpha &= \alpha_0 + \alpha'\,\xi + \alpha''\,\xi^2, \\ \beta &= \beta_0 + \beta'\,\xi + \beta''\,\xi^2, \\ \xi &\equiv \log(1+z) \end{aligned} \tag{11}$$

(note that log here and throughout refers to $\log_{10}$). We perform this fit using only our results up to redshift $z = 4$, as the HOD constraints used to build the model have to be extrapolated at higher redshifts. In Table 1, we quantify the uncertainty in each parameter; this reflects the systematic theoretical uncertainties shown in Fig. 2 (the shaded range), with the appropriate covariance between parameters taken into account (for this reason, fitting the redshift evolution with free parameters up to second order in ξ leads to relatively large uncertainties in the fit results). We also illustrate the best-fitting parameters as a function of redshift in Fig. 3.

The behaviour seen in each parameter reflects that discussed above; the bright and faint-end slopes, and normalization ϕ_*, evolve relatively weakly with redshift.[6] In fact, we can find reasonable fits within the theoretical uncertainties that hold these parameters fixed with redshift. But, the break luminosity L_* evolves rapidly, as $\propto(1+z)^2$ for $z < 2$ in all populations, then levels out to a maximum at higher redshifts. We do see this flattening from $z \sim 2$ to 4, hence the quadratic term here; although given our $z < 4$ limit [$\log(1+z) < 0.7$], we are only just sensitive to the quadratic terms in ξ (and see no significance fitting higher order terms).

At all redshifts, L_* is higher for merger/AGN populations ($>10^{12}\,{\rm L}_{\odot}$) relative to normal galaxies; but the space density ϕ_* is much lower (by a factor of ∼100–300). The bright-end slope of the normal population is steep, reflecting the rapid exponential cut-off in the galaxy MFs; the bright-end slope in the merger/AGN populations is much more shallow, ∼ 2.5–3 – such a slope is, in fact, very similar to the observed bright-end slope of the brightest IR populations (Sanders et al. 1988a, 1990; Chapman et al. 2005) and to the well-constrained bright-end slope of the quasar LFs from redshifts $z \sim 0$ to 6 (see e.g. Fan et al. 2004; Brown et al. 2006; Richards et al. 2006b; Hopkins et al. 2007c; Shankar et al. 2009; Croom et al. 2009, and references therein).

For comparison, we also consider fitting the LFs to a modified Schechter function parameterization, namely

$$\Phi = \phi_* \left(\frac{L}{L_*}\right)^{-\alpha} \exp\left[-\left(\frac{L}{L_*}\right)^{\beta}\right], \tag{12}$$

with the same assumed form for the evolution in the fit parameters with redshift. This is akin to a standard Schechter function except

[6] The apparent 'jump' in ϕ_* at $z \approx 0.3$ owes partly to real evolution in the observed input MFs, but mostly to parameter covariance (here between ϕ_*, L_* and α). Accounting for this covariance, the change in ϕ_* from $z = 0.2$ to 0.3 is only significant at 1.5σ–2σ, and a smoothly evolving ϕ_* provides just as good a fit.

Table 1. Fits to model IR LF predictions.

Object class[a]	$L_0(\pm\,\Delta L_0)^b$	L'^c	L''^d	$\phi_0{}^e$	ϕ'^f	ϕ''^g	$\alpha_0{}^h$	α'^i	α''^j	$\beta_0{}^k$	β'^l	β''^m
Double-power-law fit (full) – standard model												
Normal/Star-forming	11.37(0.14)	2.17(0.82)	−1.15(1.13)	−3.97(0.50)	5.27(2.81)	−6.11(3.53)	1.57(0.45)	−3.40(2.46)	2.09(3.06)	6.60(1.33)	7.46(8.12)	−17.57(10.81)
Merger/burst	12.16(0.26)	1.93(1.53)	−2.41(2.09)	−6.35(0.52)	5.15(3.06)	−4.77(4.02)	1.13(0.21)	−0.86(1.30)	0.30(1.76)	3.23(0.59)	3.94(3.55)	−7.42(4.69)
Obscured AGN	12.15(0.29)	2.07(1.63)	−3.19(2.10)	−6.62(0.47)	5.69(2.56)	−5.39(3.15)	0.73(0.23)	−0.64(1.37)	−0.83(1.85)	2.55(0.50)	3.90(2.91)	−7.41(3.74)
Double-power-law fit (first-order in z) – standard model												
Normal/Star-forming	11.31(0.12)	1.99(0.29)	0	−3.30(0.41)	0.16(0.88)	0	1.39(0.35)	−1.68(0.72)	0	6.59(1.10)	0.95(3.44)	0
Merger/Burst	12.08(0.30)	1.23(0.69)	0	−5.67(0.59)	0.72(1.33)	0	1.07(0.25)	−0.53(0.55)	0	3.18(0.60)	0.79(1.71)	0
Obscured AGN	11.95(0.34)	1.37(0.75)	0	−5.80(0.53)	0.76(1.11)	0	0.69(0.28)	−0.83(0.60)	0	2.40(0.45)	1.06(1.32)	0
Modified Schechter function fit – standard model												
Normal/Star-forming	10.46(0.58)	2.35(0.97)	0	−1.64(0.70)	−1.28(1.14)	0	0.46(0.74)	−0.99(1.24)	0	0.73(0.22)	0.25(0.40)	0
Merger/burst	10.23(1.83)	1.05(0.64)	0	−3.41(1.10)	0.21(0.57)	0	0.28(0.72)	−0.26(0.76)	0	0.36(0.15)	0.0(0.0)	0
Obscured AGN	10.10(0.66)	0.90(0.60)	0	−4.25(0.40)	−0.36(0.81)	0	0.0(0.0)	−0.60(0.61)	0	0.33(0.06)	0.0(0.0)	0
Double-power-law fit (full) – steeper Kennicutt–Schmidt index												
Normal/Star-forming	11.28(0.14)	2.43(0.84)	−1.12(1.14)	−4.09(0.53)	5.67(2.91)	−6.35(3.58)	1.69(0.48)	−3.93(2.55)	2.48(3.09)	6.57(1.36)	7.39(8.12)	−17.75(10.66)
Merger/burst	12.39(0.25)	2.06(1.49)	−2.59(2.07)	−6.61(0.45)	5.00(2.65)	−4.84(3.52)	0.96(0.17)	−0.85(1.05)	0.48(1.43)	2.93(0.50)	3.71(3.08)	−6.88(4.09)
Obscured AGN	12.15(0.29)	2.07(1.63)	−3.19(2.10)	−6.62(0.47)	5.69(2.56)	−5.39(3.15)	0.73(0.23)	−0.64(1.37)	−0.83(1.85)	2.55(0.50)	3.90(2.91)	−7.41(3.74)
Modified Schechter function fit – steeper Kennicutt–Schmidt index												
Normal/Star-forming	10.34(0.56)	2.79(0.91)	0	−1.62(0.69)	−1.34(1.11)	0	0.51(0.71)	−1.07(1.16)	0	0.72(0.21)	0.27(0.38)	0
Merger/burst	10.62(1.53)	1.05(0.59)	0	−3.83(0.95)	0.30(0.51)	0	0.27(0.53)	−0.21(0.59)	0	0.36(0.13)	0.0(0.0)	0
Obscured AGN	10.10(0.66)	0.90(0.60)	0	−4.25(0.40)	−0.36(0.81)	0	0.0(0.0)	−0.60(0.61)	0	0.33(0.06)	0.0(0.0)	0
Double-power-law fit (full) – no gas fraction evolution												
Normal/Star-forming	11.38(0.15)	1.06(0.96)	−1.50(1.41)	−4.00(0.57)	4.36(3.45)	−5.71(4.65)	1.57(0.53)	−2.12(3.36)	1.05(4.67)	6.70(1.52)	7.34(9.66)	−16.84(13.18)
Merger/Burst	12.20(0.26)	1.35(1.54)	−2.77(2.12)	−6.40(0.53)	4.51(3.18)	−3.53(4.26)	1.12(0.22)	−0.21(1.42)	−0.58(2.05)	3.33(0.64)	4.08(3.85)	−7.61(5.03)
Obscured AGN	12.15(0.33)	1.91(1.92)	−2.88(2.62)	−6.60(0.51)	5.45(2.99)	−5.29(3.90)	0.75(0.24)	−0.83(1.48)	0.33(2.04)	2.54(0.53)	3.65(3.20)	−6.66(4.23)
Modified Schechter function fit – no gas fraction evolution												
Normal/Star-forming	10.37(1.08)	0.93(1.74)	0	−1.52(0.94)	−1.55(1.47)	0	0.27(1.48)	−1.01(2.53)	0	0.69(0.34)	0.18(0.61)	0
Merger/burst	10.09(2.41)	0.18(0.74)	0	−3.41(1.12)	0.58(0.61)	0	0.18(0.92)	−0.15(0.94)	0	0.35(0.19)	0.0(0.0)	0
Obscured AGN	10.07(0.71)	0.73(0.68)	0	−4.31(0.41)	0.38(0.61)	0	0.0(0.0)	−0.28(0.65)	0	0.32(0.06)	0.0(0.0)	0

[a]Refers to subsample of objects for which the fit pertains.
[b]Parameters of best fit to the redshift-dependent form of the IR LF (equations 10–12). L_0 is the break luminosity L_* at $z = 0$, in $\log(L_0/\mathrm{L}_\odot)$.
[c–d]Redshift dependence of the break luminosity L_*, per equation (11) [$\log(L_*/\mathrm{L}_\odot) = L_0 + L'\,\xi + L''\,\xi^2$, where $\xi \equiv \log(1+z)$.]
[e]Log LF normalization ϕ_* at $z = 0$, in $\mathrm{Mpc}^{-3}\,\log^{-1} L_{\mathrm{IR}}$.
[f–g]Dependence of normalization ϕ_* on redshift ($\log\{\phi_*/\mathrm{Mpc}^{-3}\,\log^{-1}\,L_{\mathrm{IR}}\} = \phi_0 + \phi'\,\xi + \phi''\,\xi^2$).
[h]Faint-end IR LF slope α at $z = 0$.
[i–j]Dependence of faint-end slope α on redshift ($\alpha = \alpha_0 + \alpha'\,\xi + \alpha''\,\xi^2$).
[k]Bright-end IR LF slope β at $z = 0$.
[l–m]Dependence of bright-end slope β on redshift ($\beta = \beta_0 + \beta'\,\xi + \beta''\,\xi^2$).
Observed galaxy MFs extend to $z \approx 4$, the range used for these fits. Extrapolations beyond this redshift should be considered with caution.
If this is done, however, a minimum should be imposed on the bright-end slope at $\beta \gtrsim 2$.

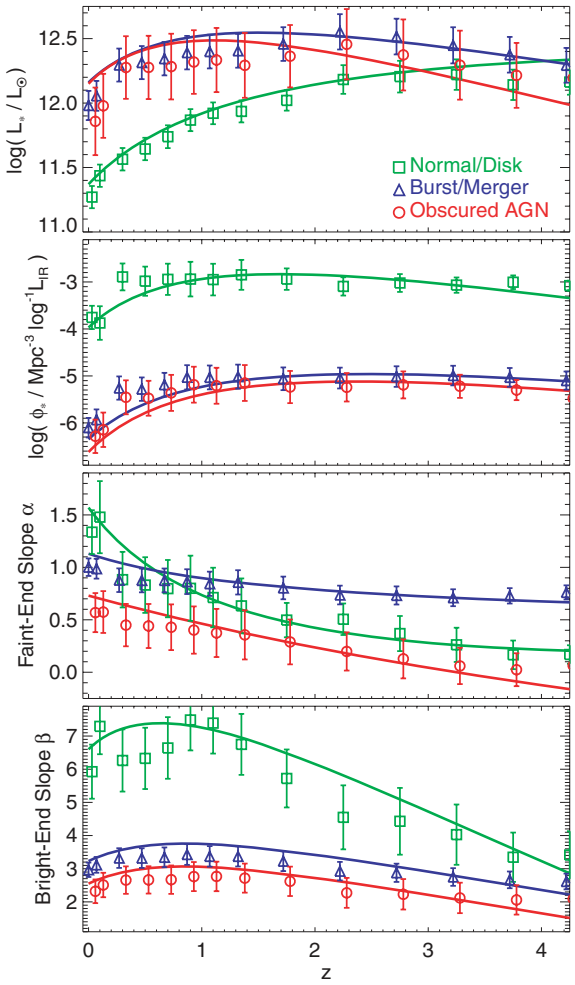

Figure 3. Best-fitting parameters for the LFs in Fig. 2, given a double-power-law formulation (equation 10). Points show the best fit (with uncertainty reflecting the allowed range in Fig. 2) at several redshifts, lines the overall maximum likelihood fits from Table 1. Parameter degeneracies are such that the best-fitting curves can be systematically slightly offset from the fits at each redshift. Top panel: break luminosity. Rising gas fractions drive the increase; but for mergers, the results asymptote to a maximum owing to the physics of very gas-rich mergers (see the text). Second from top panel: normalization. Modulo a decrease at the lowest redshifts, this is approximately redshift independent. Second from bottom panel: faint-end slope. Again, the redshift dependence is weak. The apparent large evolution for star-forming systems is somewhat degenerate with the evolution in the bright-end slope – a fit where both are held constant is, in fact, acceptable. Bottom panel: bright-end slope. Again, relatively flat with redshift (per note above). Star-forming systems fall off in number density at high luminosities much more steeply than mergers or quasars, reflecting the exponential cut-off in the MF.

with the addition of a bright-end 'slope' term β, where $\beta < 1$ allows for a less-steep falloff at high L than would be predicted by a standard Schechter function ($\beta = 1$). We find that, because the functions shown in Fig. 2 do not have sharp 'breaks' characteristic of a double power-law, this provides a marginally more accurate representation of the LF *shape*. However, the difference is small, and direct interpretation of the parameters in equation (12) is complicated by serious fitting degeneracies. With this choice of functional form, we find the second-order redshift evolution terms make little difference to the fits, and so – given the steep parameter degeneracies involved – do not free the higher order terms in the fit. Interestingly, the *total* LF obtained by summing the contributions from each component is better represented with a double power law, as opposed to the modified Schechter function.

3.3 The luminosities and space densities of population transitions

We explicitly quantify the 'transition point' between the dominance of one population or another as a function of redshift in Fig. 4. Specifically, we define this as the point where the LFs from different populations in Fig. 2 cross. For example, the transition luminosity or space density between dominance by normal discs and mergers is given by the point in Fig. 2, where $\phi(L_{\rm IR} \mid {\rm normal}) = \phi\,(L_{\rm IR} \mid {\rm burst})$; above this $L_{\rm IR}$ [and below the corresponding $\phi(L_{\rm IR})$], $\phi(L_{\rm IR} \mid {\rm burst}) > \phi(L_{\rm IR} \mid {\rm normal})$, at lower luminosities and higher space densities the opposite is true. Likewise, we can define the transition luminosity or space density where obscured AGN become numerous than star formation dominated systems, $\phi\,(L_{\rm IR} \mid {\rm AGN}) = \phi(L_{\rm IR} \mid {\rm normal}) + \phi(L_{\rm IR} \mid {\rm burst})$. The uncertainties in Fig. 2 are translated to corresponding uncertainties here.

Our comparisons generally affirm the conventional wisdom: at low redshift, mergers dominate the ULIRG and much of the LIRG populations, above a luminosity $\sim 10^{11.5}\,{\rm L}_{\odot}$. Heavily obscured (potentially Compton-thick) AGN (in starburst nuclei) become a substantial contributor to IR luminous populations in the most extreme

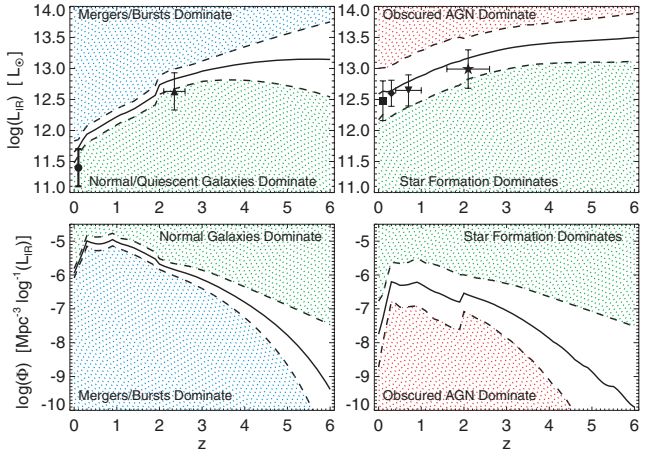

Figure 4. Top-left panel: total IR luminosity threshold above which the predicted IR LFs in Fig. 2 transition from being dominated by non-merging (quiescent) discs to merger-induced star formation/bursts. We compare observational estimates from morphological studies of bright-IR sources in Sanders & Mirabel (1996, circle) and Tacconi et al. (2008, triangle). Bottom-left panel: same, but showing the space density threshold (Φ, in ${\rm Mpc}^{-3}\,{\rm log}^{-1}\,L_{\rm IR}$) of the same transition. Top-right panel: luminosity threshold above which the IR LFs transition from being dominated by star formation to being dominated by AGN. Points show the observed estimates from comparison of PAH feature strengths and emission line strength template fitting in Chary & Elbaz (2001, square), Veilleux et al. (2009b,a, diamond), and Sajina et al. (2007, star) and from comparison of the far IR-radio correlation in Yang et al. (2007). Bottom-right panel: same, in terms of the space density threshold. As gas fractions increase with redshift, SFRs increase in all systems. As a result, the threshold for merger dominance grows from bright LIRGs at $z \sim 0$, to bright ULIRGs at $z \sim 1$–2, to HyLIRGs at $z > 2$. In terms of space density, this transition is relatively constant over this range at 10^{-6}–$10^{-5}\,{\rm Mpc}^{-3}\,{\rm log}^{-1}\,L_{\rm IR}$ (at higher redshifts, the space densities of all massive systems drop rapidly). At all redshifts, bright HyLIRGs ($L_{\rm IR} \gg 10^{13}\,{\rm L}_{\odot}$; $\Phi \sim 10^{-7}\,{\rm Mpc}^{-3}\,{\rm log}^{-1}\,L_{\rm IR}$ at $z \sim 0$–4) have a non-negligible AGN contribution.

$\gtrsim$ a few $\times$ $10^{12}\,L_\odot$ systems (nearing HyLIRG $>10^{13}\,L_\odot$ luminosities which are common bolometric luminosities for $>10^8\,M_\odot$ BHs near Eddington, but would imply potentially unphysical $\gtrsim$ $1000\,M_\odot\,yr^{-1}$ SFRs). At higher redshifts, discs are more gas-rich, and thus have characteristically larger SFRs, dominating the IR LFs at higher luminosities. By $z\sim1$, most LIRGs are quiescent systems, and by $z\sim2$ only extreme systems $\gtrsim$a few $\times$ $10^{12}\,L_\odot$ are predominantly mergers/AGN.

This appears to agree well with recent observations. First, consider the results of systematic morphological studies of IR-bright sources as a function of their luminosities, at low redshifts (Sanders & Mirabel 1996), which affirms the conclusion that – locally – the brightest LIRGs and essentially all ULIRGs are merging systems, while less-luminous systems are not (see also references in Section 1). At high redshifts, similar studies have now been performed (see e.g. Tacconi et al. 2008, and references therein). They too find that the brightest sources are almost exclusively mergers, but with a transition point (from non-merger to merger dominated) an order-of-magnitude larger in luminosity. Other morphological studies at intermediate redshifts $z\sim0.4$–1.4 have reached similar conclusions (Bridge et al. 2007).

Other studies have attempted to separate the contributions of star formation and (obscured) AGN. At low redshifts, we find similar results from observational comparison of emission line strengths (Sanders & Mirabel 1996; Kewley et al. 2006), observations of the strength of observed PAH features (Lutz et al. 1998; Veilleux et al. 2009b), full SED template fitting (Farrah et al. 2003) or indirect comparison with type 2 AGN LFs (Chary & Elbaz 2001). In each case, these studies find that local 'normal' ULIRGs are star formation dominated, but extremely rare systems approaching HyLIRG luminosities tend to be AGN dominated. At high redshifts, there have recently been attempts to apply similar methodologies, especially comparison of PAH strengths, and we show such an estimate from Sajina et al. (2007), who find a similar transition from star formation to AGN dominance as at low redshift, at a factor of several higher luminosity. Yang et al. (2007) measure dust temperature distributions and positions on the far IR-radio correlation for a sample of ULIRGs over the redshift range $z=0.3$–1; they find that below $L_{\rm IR}=10^{12.4}\,L_\odot$ ($L_{\rm FIR}=10^{12.25}\,L_\odot$) the systems appear star formation dominated, while above $L_{\rm IR}=10^{12.9}\,L_\odot$ the IR luminosities are dominated by AGN. At $z=2$, the same constraints support the conclusion from Sajina et al. (2007); Younger et al. (2009b) show that samples of $\sim$2–8 $\times$ $10^{12}\,L_\odot$ ULIRGs at $z=2$ follow the local far-IR–radio correlation, indicating they are starburst dominated, but Bussmann et al. (2009a,b) find that by luminosities of $\sim2\times10^{13}\,L_\odot$ IR samples are dominated by warm dust sources more likely to be (post-merger) AGN. Of course, changing the assumed number of obscured AGN, as a function of luminosity or redshift, will correspondingly shift the predicted transition point; the agreement seen here suggests that the correct number is probably not very different from that adopted here. For further details, we refer to the above as well as Chapman et al. (2005), Dey et al. (2008) and Casey et al. (2009).

The transition point between non-merger and merger dominance of the LF shifts to larger luminosities at high redshifts, even though gas-rich merger rates increase rapidly. The evolution in gas fractions, which drives up both disc SFRs and merger-induced bursts similarly, is the dominant effect; the evolution in merger rates is also not *so* rapid as to dominate the population at redshifts $z\lesssim2$. Moreover, as noted in Section 2, although disc SFRs (at otherwise fixed properties) increase monotonically with their gas fractions and hence gas surface densities, merger-induced bursts and quasar episodes can decline in efficiency in extremely gas-rich systems, because the gravitational torques that allow for such bursts depend on a sizable dissipationless (stellar) disc component (Hopkins et al. 2009b). As a result, merger-induced bursts do not grow in importance as rapidly as might naively be expected from analysis of, for example, halo–halo merger rates.

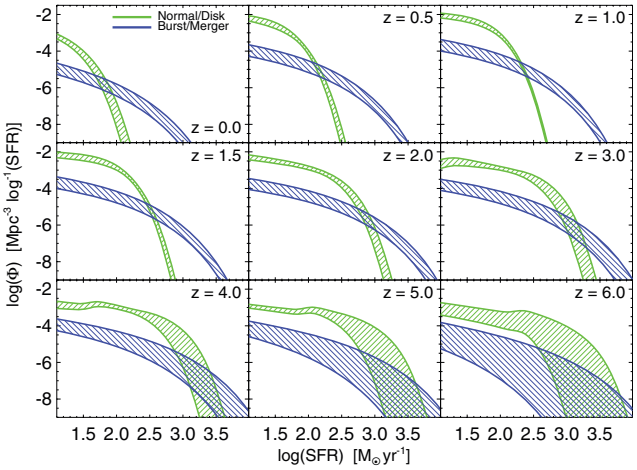

Figure 5. As Fig. 2, but showing the distribution of SFRs at each redshift (hence no AGN contribution).

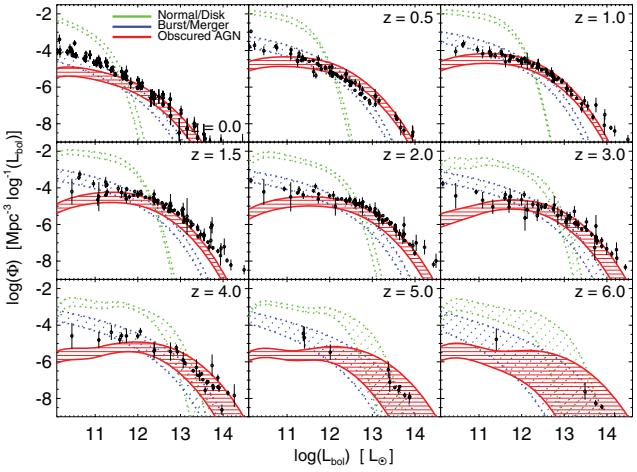

Figure 6. As Fig. 2, but in terms of bolometric luminosity (similar to the IR for star-forming systems, but significantly larger for AGN, which are highlighted here). Black points show the compilation of observational data used to derive bolometric AGN LFs in Hopkins et al. (2007c); these should be compared to the predicted AGN LF.

3.4 Corresponding SFRs and bolometric luminosities

In Fig. 5, we reproduce our model from Fig. 2, but show instead the distribution of SFRs. Of course, AGN are not present here, since although there will be star formation in their hosts, the AGN IR luminosity itself is not from star formation.

Fig. 6 shows the corresponding bolometric LFs. For the star-forming systems, this is essentially identical to the total-IR LFs, as the total IR emission dominates the bolometric luminosity in at least the luminous, IR-bright end of the distribution (of interest here). However, for the AGN, the bolometric emission is considerably larger than the IR emission. We therefore highlight the AGN predictions. We compare these to the large compilation of

observations used to derive bolometric quasar LFs in Hopkins et al. (2007c) (see references therein). Similar results have been obtained in other compilations (Shankar et al. 2009), or from hard X-ray LFs with appropriate bolometric corrections (see e.g. Yencho et al. 2009; Aird et al. 2010). The observationally estimated bolometric QLF agrees reasonably well with our predictions. The underprediction of very low-luminosity AGN owes to our neglect of non-merger induced AGN (Section 2.4); it is clear here that these have a negligible impact on our conclusions. The model may also somewhat underpredict the number density of the most luminous systems ($L_{\rm bol} > 10^{14}\,L_{\odot}$); this is discussed in detail in Hopkins et al. (2008d), but is sensitive to the assumed scatter in bolometric corrections and to the existence of even a small lensed or beamed QSO population.

3.5 The effects of different model assumptions

We briefly outline the effects of several important components in the models adopted. For further details, see Appendix B, where we reproduce our model from Fig. 2 explicitly, with different changes (discussed here) to the model.

If we do not allow galaxy gas fractions to evolve with redshift (i.e. adopt the $z = 0$ value at all redshifts), this leads to a substantial underprediction of the luminosities of 'quiescent' galaxies at $z \geq 1$. In short, the existence of apparently 'normal' galaxies at high redshifts, with ULIRG-level luminosities, requires very high gas surface densities (relative to those at $z = 0$) if the Kennicutt (1998) relation is to hold in some form.

If we do not allow for disc sizes to be more compact at high redshift, this yields lower surface densities, and hence somewhat lower SFRs, but the effect is relatively minor. Because the observed size evolution (of star-forming galaxies) is weak [$R_e(M_*) \propto (1+z)^{-(0-0.6)}$] and the size evolution (at otherwise fixed properties) only enters into the SFR at sublinear order (for $\dot{\Sigma}_* \propto \Sigma_{\rm gas}^{1.4}$, this yields $\dot{M}_* \propto R^{-0.8}$ at otherwise fixed properties), the total difference is relatively small (a factor of $\sim$2) in luminosity, comparable to many of the other uncertainties involved.

If we do not allow for scatter in any quantities (e.g. disc sizes, gas fractions, burst masses, quasar bolometric corrections and SFRs at otherwise fixed properties) – i.e. force all values to exactly trace the medians given in Section 2 – this has the expected effect, that the rare, high-L population is significantly suppressed. These objects depend on the existence of some systems with relatively high gas fractions at high masses and high $L_{\rm IR}$ relative to many of their other properties.

We can also reconstruct our model predictions, but adopt a more steep power-law index for the Kennicutt (1998) relation, for example $\dot{\Sigma}_* \propto \Sigma_{\rm gas}^{1.6}$, as suggested by some recent observations of high-redshift systems (Bouché et al. 2007). In order to avoid overproducing local SFRs (and indeed the LFs at all luminosities and redshifts), it is necessary to correspondingly renormalize the relation: we do so such that a Milky Way like disc, with effective gas surface density $\approx 3 \times 10^8\,M_{\odot}\,{\rm kpc}^{-2}$ (10 per cent gas fraction), has the same SFR as that expected from the relation fit by Kennicutt (1998). This amounts to a factor of $\approx$3.1 lower normalization in equation (3), with the steeper n_K. Considering simulations with such a steeper index, the resulting burst properties are qualitatively similar, but the burst time-scale in equation (6) is shorter by a factor of $\approx$2, $t_{\rm burst} \approx 0.4 \times 10^8$ yr. The AGN properties are relatively unchanged. Together, the results from this revised model are similar to our default model – however, the steeper index leads to more star formation in the very high gas density systems at high redshift. This actually somewhat improves the agreement with the observed number densities of the most luminous systems; however, the difference is ultimately within the range of our other uncertainties, in particular the number density of the most massive galaxies.

Again, to facilitate future comparisons, we provide in Table 1 fits to the same double-power-law functional form for the predicted LFs in both the case of no gas fraction evolution and the case of a steeper Kennicutt–Schmidt index.

3.6 The luminosity/SFR density: contribution of mergers and AGN

3.6.1 Luminosity densities: predictions

In Fig. 7, we examine the distribution of SFRs at fixed galaxy stellar mass (for an $\sim L_*$, $M_* = 10^{11}\,M_{\odot}$ system), for the standard model used in constructing Fig. 2, at $z = 0$ and 2. We separately show the distribution of SFRs from the 'quiescent' (non-merger) systems at that mass, and from the merger-induced bursts. The scatter in non-merger systems comes from the distribution of gas fractions and effective radii, at a given stellar mass and redshift. Obviously, SFRs

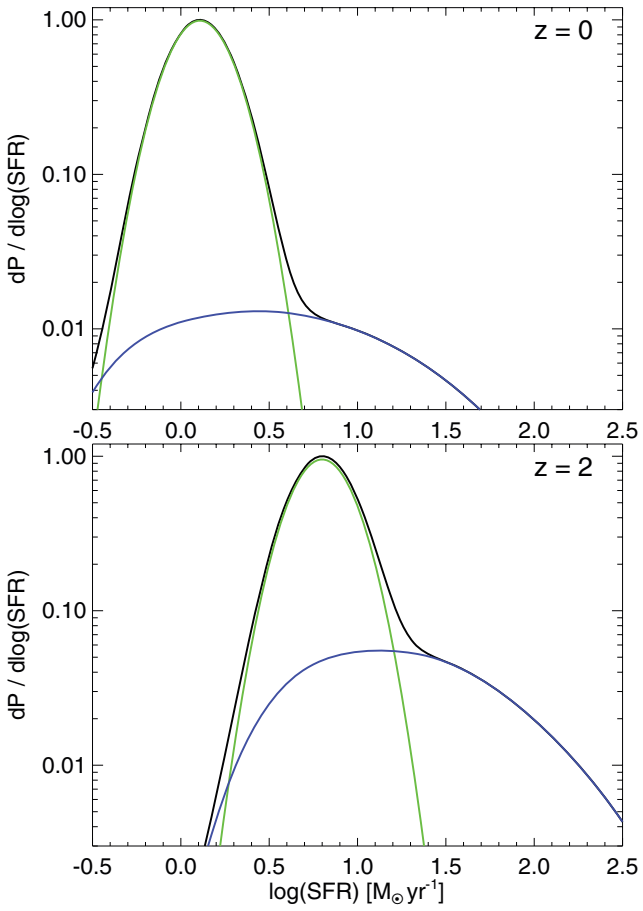

Figure 7. Distribution of SFR in galaxies of fixed mass ($M_* = 10^{11}\,M_{\odot}$) at $z = 0$ and 2. We show the total (black), contribution from 'normal' systems (green) and contribution from merger-induced bursts (blue). The 'normal' systems here have scatter reflecting that in their radii and gas fractions (assumed lognormal). Mergers, even at $z = 2$, do not dominate the population or scatter in SFR(M_*), except in the extreme wings, consistent with observations indicating small deviations about the median M_*–SFR trend in normal galaxies (Noeske et al. 2007a). Observations probing between $\sim 2\sigma$ and 3σ in the wings are needed to see the merger 'tail.'

are systematically higher at $z = 2$, and the merger contribution is relatively larger, as merger fractions observed have increased from $\sim$1 per cent at $z = 0$ to $\sim$10 per cent at $z = 2$ (see e.g. Kartaltepe et al. 2007; Lin et al. 2008; Bluck et al. 2009; Bundy et al. 2009; Conselice, Yang & Bluck 2009; Hopkins et al. 2009g; Bridge et al., in preparation; Jogee et al. 2009, and reference therein). However, at both redshifts, the merger contribution is relatively small, and although it dominates the tail at very high SFR at fixed mass it constitutes much less than the >30 per cent of the population needed for it to bias the $\sim 1\,\sigma$ scatter in SFR(M_*). Various observations have shown that there is a tight sequence of SFR with galaxy mass in star-forming systems (e.g. Noeske et al. 2007a), with small scatter $\lesssim$0.3 dex, similar to that predicted here. This presents a constraint on the role of merger-induced bursts in affecting SFRs, but one easily satisfied here – far from affecting the scatter at the 1σ level, one has to observe the scatter at a level between 2 and 3σ in the high-SFR 'wings' of the distribution at fixed stellar mass before the merger-induced tail would be evident.

Fig. 8 combines the LFs predicted in Fig. 2 to show the total IR luminosity density, and corresponding total SFR density, of the Universe as a function of redshift. Approximate fits to these predictions can be obtained by simply integrating the fitted LFs in Table 1. The luminosity density in quiescent systems dominates the global total at all redshifts. Merger-induced bursts contribute a relatively small fraction to the global SFR density; rising from $\sim$1–5 per cent at low redshifts $z \sim 0$ to a roughly constant $\sim$4–10 per cent at $z > 1$.

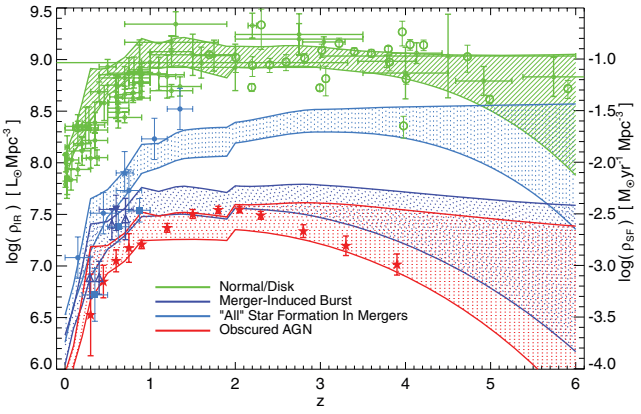

Figure 8. Total IR luminosity density (and corresponding SFR density) as a function of redshift. We show the model prediction for the contribution from 'normal' (non-merger-induced) disc star formation (green), and that for merger induced bursts (dark blue), and AGN (red), as in Fig. 2. We also show the total IR luminosity density associated with 'ongoing' interactions, which might be identified via morphology or pair-selected samples for a duration $\sim$1 Gyr (light blue). Note that most of the star formation in these systems is the continuation of their 'quiescent' star formation – the specifically merger-induced starburst lasts $\sim 10^8$ yr. We compare the observational compilation from Hopkins & Beacom (2006) for the total IR luminosity density/SFR density (green diamonds) and at high redshifts the SFR density inferred from Lyman α forest measurements in Faucher-Giguère et al. (2008, green circles). We also compare the results from the multiwavelength 'bolometric' AGN LF compilation from Hopkins et al. (2007c) for the IR luminosity density in AGN (red). Observational estimates of the SFR density specifically *induced* by mergers (e.g. subtracting some 'baseline' SFR estimate from a control sample of non-merging systems for identified mergers) are shown (dark blue) from Jogee et al. (2009, triangles) and Robaina et al. (2009, inverted triangle); estimates of the total SFR density in ongoing/identifiable (e.g. pair or morphologically selected) mergers are shown (light blue) from Menanteau et al. (2006, circles), Brinchmann et al. (1998, squares) and Bell et al. (2005, star). At all redshifts, AGN represent a small contribution to the total (FIR-dominated) IR luminosity density. Merger-*induced* star formation is a similarly small $\sim$5 per cent of the IR luminosity density; the *total* luminosity density associated with mergers is somewhat larger, but still small, rising from $\sim$5–10 per cent at $z < 1$ to $\sim$10–20 per cent at $z \sim 2$–4.

The contribution from obscured AGN is at most comparable to that from merger-induced bursts, and in general a factor of $\sim$2–3 lower (of course, the conversion to SFR density is not valid for AGN, as the IR emission is powered by accretion; they should be compared to the total IR luminosity density only). It is unlikely that obscured AGN contribute more than $\sim$5 per cent to the global IR luminosity density, even assuming a generous near-isotropically obscured fraction of $\sim 1/2$ at high luminosities (large given the observational constraints from e.g. Daddi et al. 2007; Gilli, Comastri & Hasinger 2007; Hickox et al. 2007; Tajer et al. 2007; Caccianiga et al. 2008; Treister, Krolik & Dullemond 2008; Malizia et al. 2009; Menéndez-Delmestre et al. 2009; Treister et al. 2009; Trichas et al. 2009). In fact, allowing the entire *bolometric* AGN luminosity density estimated in Hopkins et al. (2007c) and Shankar et al. (2009) to be reradiated in the IR increases the contribution of AGN by only a factor of $\sim$3. Even under conservative assumptions, then, the contribution from obscured AGN is much less than the other current statistical and systematic errors in the estimation of the global SFR density, and IR-derived SFR densities are not likely to be significantly contaminated by AGN. This question has been studied via other means, as well – e.g. in X-ray background synthesis models – with similar conclusions (see e.g. Treister & Urry 2006; Treister et al. 2008).

These are global statements – at a given (high) luminosity, the contribution of merging systems and/or AGN may be much higher. Moreover, at any specific frequency, the results here could be quite different – e.g. in near and mid-IR wavelengths AGN might be relatively much more luminous than cold dust emission from galaxy-wide starbursts (and even unobscured AGN will contribute significantly at these wavelengths), thus the AGN luminosity density in such a rest-frame band might compete with or dominate the luminosity density from star formation (see e.g. Blain et al. 1999).

As discussed in Section 2, there is an important difference between the total SFR density specifically *induced* via merger-driven galaxy starbursts (i.e. gas losing angular momentum owing to gravitational processes in the merger, falling to the galaxy centre, and driving a short-lived starburst over $\sim 10^8$ yr time-scales), and the total SFR density that might be identified observationally as 'in ongoing mergers'. The latter includes all star formation in systems that would be identified as merging (usually specifically limited to 'major' mergers), via either some morphological or pair-separation based selection criteria. The duration of these phases (and hence the total SFR density associated with mergers in such a manner) depends on the exact selection criteria, but calibration of observational methodologies with numerical simulations suggests it is $\sim$1 Gyr (see e.g. Lotz et al. 2008). During this time, except for the much shorter duration of the burst itself, the SFRs will (to lowest order, at least) reflect the 'quiescent' or 'normal' SFR of the discs, appropriate for their gas content and structural properties (see e.g. di Matteo et al. 2007; Cox et al. 2008; Cox et al., in preparation). In order to compare with these observations, we calculate the analogous SFR density in ongoing mergers with the following simple method: given the total rate of major mergers at each redshift, we simply assume a 1 Gyr observable lifetime for each such (major, $\mu > 1/3$) merger, and during this time assume it has a constant SFR equal to the rate of the quiescent systems with the same properties. We add

the SFR density calculated in this fashion to that from the bursts themselves, and obtain an estimate of the 'total' SFR that might be associated with, for example, disturbed or paired systems.

This is much larger than the burst SFR density, especially at high redshifts. At high redshifts, merger rates are high, so a long observable duty cycle ∼1 Gyr means that a large fraction of systems will appear perturbed (i.e. the 'merger fraction' will become large), and so a large fraction of star formation will appear in mergers. Here, we estimate this to rise from a few per cent at $z = 0$ to ∼20 per cent at $z \sim 2$ and as high as ∼20–50 per cent at $z \sim 3$–6. This is similar to the conclusions from the analysis in Hopkins et al. (2006c), using a different methodology but similarly attempting to calculate the total SFR in 'ongoing' mergers. Of course, this should be larger than the burst SFR density at all times; but, the primary reason the difference becomes so large at high redshift is that typical gas fractions are very large. As discussed in Section 2, and shown in detail in simulations in Hopkins et al. (2009b,f), large gas fractions lead to less efficient angular momentum loss and so (relatively) less efficient bursts in mergers, on average. However, local star formation in discs is not affected by this; SFRs in the 'quiescent' or extended disc mode continue to rise superlinearly with $f_{\rm gas}$ according to the Kennicutt (1998) law.

3.6.2 Luminosity densities: comparison with observations

We compare these predictions to a number of observational constraints. First, for the total luminosity/SFR density, we show the compilation of observations presented in Hopkins (2004) and Hopkins & Beacom (2006). These come, for the SFR density, from a variety of different observations at various wavelengths; they are shown here in terms of the estimated total SFR density with the IR luminosity density following from the standard conversion adopted here. Complementary constraints at higher redshift can be inferred from observations of the Lyman α forest in quasar spectra and ionizing background, compiled in Faucher-Giguère et al. (2008). At all redshifts, the prediction is within the scatter of these observations; at low redshifts $z \lesssim 1$, the median predicted is somewhat higher than the median of the observed points but the difference is small in absolute terms, ∼0.2 dex – well within the systematic uncertainties of both theory and observations.

Next, we consider the luminosity density in obscured AGN. Hopkins et al. (2007c) present bolometric quasar LFs, compiled from observations at a wide range of different wavelengths, together with observationally inferred column density distributions and template spectra. Adopting the fits therein,[7] assuming that the obscured luminosity is reradiated in the FIR, we construct the corresponding QSO IR luminosity density. This agrees well with our theoretical estimate. Similar constraints are obtained from the complimentary QLF compilations presented in Shankar et al. (2009) and from synthesis models of the IR backgrounds (e.g. Blain et al. 1999).

We also compare observational estimates of the luminosity/SFR density in mergers. First, several authors have attempted to estimate the total amount of star formation in observationally identified ongoing mergers or recent (morphologically disturbed) merger remnants. We compare observations compiled from Brinchmann et al. (1998), Menanteau et al. (2006) and Bell et al. (2005), who estimate this quantity in morphologically selected samples at $z \sim 0$–1.5.[8] Secondly, more recently, attempts have been made to specifically isolate the merger-*induced* SFR density. Typically, in these cases, the SFR density of some merger sample (identified in a similar manner) is considered, but only after subtracting away/removing the contribution from the expected 'normal' mode star formation. In general, this is accomplished via comparison to some control sample of star-forming galaxies with similar stellar masses and redshifts. Robaina et al. (2009) attempt this from a pair-selected sample at $z \sim 0.4$–0.8; Jogee et al. (2009) consider a similar estimate from morphologically selected samples at $z \sim 0.4$–1. Clearly, the two estimates (total SFR in 'ongoing' mergers versus the SFR density *enhancement* from mergers) should be compared to the appropriate respective theoretical predictions, as discussed above. In both cases, we see good agreement. At $z \sim 1$, the observations may in fact indicate the predicted growing difference between 'all' star formation in mergers and the star formation specifically induced by mergers.

3.6.3 Contributions from LIRGs and ULIRGs

In Fig. 9, we illustrate the contributions to the luminosity density from galaxies in various luminosity intervals – specifically, non-LIRG, LIRG and ULIRG systems. For clarity, we show just the results from our best-fitting LFs in Table 1; the full allowed range scatters about these curves by ∼0.15 dex. We find the well-known result from a number of observational studies (see e.g. Le Floc'h et al. 2005): higher luminosity systems progressively dominate more of the IR luminosity density at higher redshifts. At $z = 0$, the luminosity density is dominated by relatively low-luminosity $L_{\rm IR} \sim 10^{10}\,{\rm L}_{\odot}$ systems. The contribution from LIRGs ($L_{\rm IR} > 10^{11}\,{\rm L}_{\odot}$ systems) rises rapidly from $z = 0$ to 1, such that by $z > 0.7$ or so these systems dominate the IR luminosity density. Their fractional contribution remains relatively constant, above this point. ULIRGs ($L_{\rm IR} > 10^{12}\,{\rm L}_{\odot}$) also rise rapidly in prominence, from negligible contributions to the IR luminosity density ($\lesssim$1 per cent) at low redshifts to comparable ∼20–50 per cent contributions to LIRGs at $z \sim 2$, and by $z > 3$ dominating the total IR emission. The contribution from HyLIRGs ($L_{\rm IR} > 10^{13}\,{\rm L}_{\odot}$) rises in similar fashion, but is always much less than the contribution from ULIRGs – the highest contributions we find from such systems are at $z \gtrsim 3$ at ∼1–5 per cent of the luminosity density.

These trends simply reflect the predicted (and observed) evolution in the IR LF break $\sim L_{*}$ (see Fig. 3) – i.e. the fact that all active systems become more IR luminous at high redshifts. It should be clear both from our discussion in Section 3.3, and from direct comparison with Fig. 8, that these luminosity classes do *not* necessarily represent distinct physical object classes. As we have shown, we expect most of the LIRGs at $z \sim 1$, and ULIRGs at $z > 2$, to be 'normal' star-forming systems, with their luminosities driven by increasing gas content and rapid growth.

[7] A code for generating the observed quasar LFs in various bands, based on these observations, is provided at http://www.cfa.harvard.edu/phopkins/Site/qlf.html.

[8] Note that most of these authors actually measure the *fraction* of the SFR density in or induced by mergers, not the absolute value. We convert this to an absolute density by rescaling with the observed total SFR density at the same redshift from the best-fitting observed trend presented in Hopkins & Beacom (2006). Since this agrees well with our predicted total SFR density, it makes little difference if we use that instead.

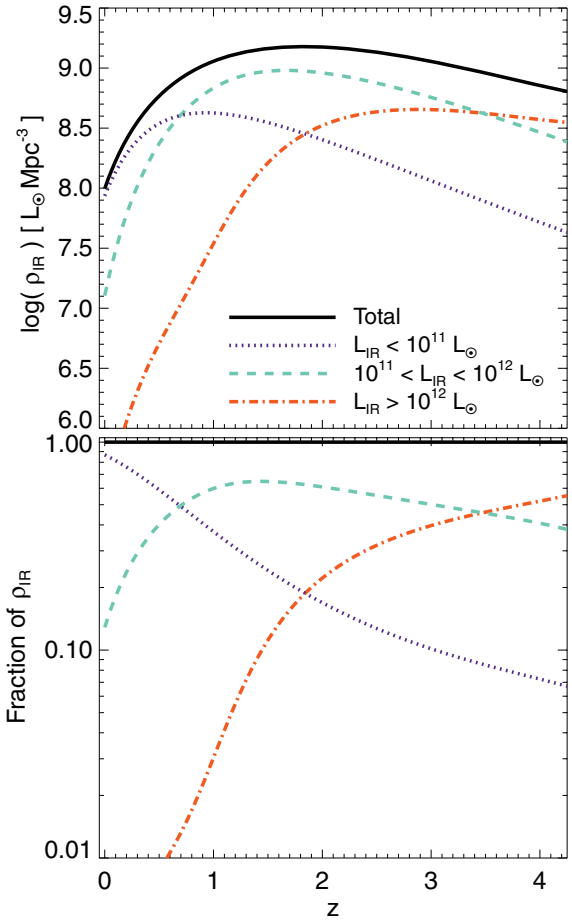

Figure 9. Contribution to the IR luminosity density from galaxies in different luminosity intervals. Top panel: luminosity density, as Fig. 8. We compare the total, and contribution from sub-LIRG ($L_{\rm IR} < 10^{11}\,{\rm L}_{\odot}$), LIRG ($L_{\rm IR} = 10^{11}$–$10^{12}\,{\rm L}_{\odot}$) and ULIRG ($L_{\rm IR} > 10^{12}\,{\rm L}_{\odot}$) systems. HyLIRGs ($L_{\rm IR} > 10^{12}\,{\rm L}_{\odot}$) are negligible ($\lesssim$1–5 per cent contribution) in this total at all redshifts. For clarity, we show the results for the fits in Table 1; each curve has an approximate 0.15 dex uncertainty. Bottom panel: same, as a fraction of the total $\rho_{\rm IR}$. LIRGs rise to dominance by $z \sim 1$. ULIRGs are comparable and then dominant in output at $z \sim 2$ and 3, respectively. We stress that, as in Fig. 4, these luminosity cuts do *not* necessarily correspond to physically different classes of systems.

4 CONCLUSIONS

We present a simple model for the distribution of SFRs and IR luminosities owing to 'normal' star-forming discs, merger-induced starbursts and AGN. Comparing this with observations, we find reasonable agreement at $z \sim 0$–3. At all redshifts, we find that the low-luminosity population is dominated by discs, whereas the high-luminosity population becomes progressively more dominated by merger-induced bursts and then, ultimately, obscured AGN.

The threshold for this transition is always at high luminosities and low space densities. At higher redshifts, gas fractions in all systems increase – hence, specific SFRs even in 'typical' systems are much higher at high z. As a consequence, the luminosity threshold for the disc–merger transition increases with redshift, from between LIRGs and ULIRGs in the local Universe, to ULIRG luminosities at $z \sim 1$, to HyLIRG luminosities at $z \sim 2$–4. Similarly, the threshold for AGN dominance, at the bright ULIRG range at low redshifts, rises to HyLIRG luminosities at $z \sim 1$–2 and to the very brightest HyLIRGs at $z > 2$.

We provide simple fitting functions for each of these quantities, and show how they depend on different parameters in the model. Most critically, it is the evolution in galaxy gas fractions that drives most of the evolution in the IR LFs. Observations have shown that typical gas fractions in massive, star-forming galaxies increase rapidly with redshift (see e.g. Erb et al. 2006; Bouché et al. 2007; Puech et al. 2008; Mannucci et al. 2009; Förster Schreiber et al. 2009). This naturally follows from the facts that cooling rates on to galaxies at high redshift are much higher than at low redshift, and there has simply been less time to process gas into stars (higher cosmic densities may also make stellar and AGN feedback relatively less efficient). A higher gas fraction by a factor of $\sim$3, as implied by observations of Milky Way mass discs at $z \sim 2$–3, leads to a factor $\sim$5–6 higher SFR, according to the Kennicutt–Schmidt relation. At high masses/luminosities, i.e. where the number density of systems is falling exponentially, such a systematic increase in luminosity more than offsets the declining space density of massive galaxies with redshift.

Other parameters have little effect. Changes in galaxy sizes and/or structural parameters, while potentially very important for, for example, how gas fractions are maintained, make little difference to the SFR distributions given some gas fraction and stellar mass distributions. Allowing for a more steep index in the Kennicutt (1998) relation may help to account for the most luminous observed systems such as bright submillimetre galaxies at the HyLIRG threshold at $z \sim 2$–4 (Chapman et al. 2005). However, the number counts of such objects remains quite uncertain, and recently it has been suggested that the average counts might be much lower with cosmic variance still a concern (Austermann et al. 2010). Larger samples and better calibration of bolometric corrections – in particular, real knowledge of the appropriate dust temperatures for conversion to total-IR luminosities, which requires sampling both sides of the cold dust peak (see e.g. Younger et al. 2009b) – will be needed for better understanding of extreme systems.

Our simple model succeeds reasonably well at explaining the observed global SFR density. At all redshifts, normal systems dominate the global SFR density. Obscured AGN contribute little, $\lesssim$5 per cent, to the total IR luminosity density. Substantial bias to IR-based SFR density estimates from obscured AGN would require an undiscovered population of heavily, isotropically obscured sources with luminosity densities approximately five times what is currently suggested (which would be in conflict with relic BH mass densities).

The contribution of merger-induced bursts is similarly small, $\sim$5–10 per cent at most redshifts. This owes both to the physics discussed above – discs also rapidly increase their SFR density with redshift owing to higher gas fractions – and also to the fact that increasing disc gas fractions arbitrarily will not continue to increase the merger-induced burst contribution arbitrarily. Rather, as discussed in detail in Hopkins et al. (2009b,f), at high gas fractions angular momentum loss in mergers becomes less efficient – thus for an otherwise identical merger with a much larger gas fraction the fraction of gas funnelled into the nuclear starburst, relative to the total available, will be less (and the fraction that remains in an extended disc distribution to continue 'normal' mode star formation will be larger), even if the absolute mass in the burst is larger. Similarly, at a given mass, the distribution of SFRs at all redshifts is dominated by normal-mode star formation – merger-induced bursts are important only in the high-SFR tail ($\sim 2\sigma$–3σ) of the distribution. These trends explain a number of recent observations that

similarly indicate a small effect of merger enhancements to SFRs, and that show that most star formation by number and luminosity density appears to follow a simple trend or 'main sequence' as a function of galaxy stellar mass and redshift (Blain et al. 1999; Bell et al. 2005; Papovich et al. 2006; Noeske et al. 2007a,b; Jogee et al. 2009; Robaina et al. 2009).

Support for these fractions also comes from completely independent sources. Recently, a number of high-resolution studies of spheroid formation via galaxy mergers have shown that properties such as the surface brightness profiles, sizes, concentrations, kinematics and isophotal shapes of spheroids are very sensitive to the mass fractions formed in such bursts, which produce dense, discy, nuclear mass concentrations, versus the mass in a more extended envelope formed via the violent relaxation of the pre-burst stellar discs (see e.g. Cox et al. 2006; Naab, Jesseit & Burkert 2006; Robertson et al. 2006; Burkert et al. 2008; Hopkins, Cox & Hernquist 2008a; Hopkins et al. 2008c; Jesseit et al. 2009; Hopkins et al. 2009c). In particular, typical $\sim L_*$ early-type galaxies, which dominate the spheroid stellar mass density, have properties that are reproduced accurately by simulations if and only if this burst fraction is $\sim$10 per cent (for details, see Hopkins et al. 2009a,e). Independent analysis of their stellar population properties leads to similar conclusions (McDermid et al. 2006; Sánchez-Blázquez et al. 2007; Reda et al. 2007; Foster et al. 2009).

There is an important technical distinction between the total SFR density in 'ongoing' or recent mergers and that actually *induced* by the merger (we present predictions for both). The former includes systems in their 'normal' star-forming mode, observable for $\sim$Gyr as perturbed or in pairs; the latter reflects specifically the $\sim 10^8$ yr event where gravitational torques drive a nuclear starburst. Under some circumstances, especially in very gas-rich mergers, the sum of this 'normal mode' star formation over a long $\sim$Gyr duration yields significantly more total stellar mass formed than in the burst itself. The 'ongoing' merger SFR density must, of course, rise with the observed merger fraction, reaching $\sim$20 per cent at $z = 2$ and as high as $\sim$20–50 per cent at $z > 4$; however, we stress that these high fractions reflect predominantly the 'normal' modes of star formation simply present in systems that may be on their way to merging.

Finally, we caution that the above comparisons are approximate, and intended as a broad means of comparing the primary drivers of star formation and their contributions relative to observed IR LFs and SFR distributions. We have ignored a number of potentially important effects: for example, obscuration is a strong function of time in a merger, and may affect various luminosities and morphological stages differently. Moreover, our simple linear addition of the star formation contribution of mergers to the IR LF and the AGN contribution is only technically correct if one or the other dominates the IR luminosity at a given time in the merger; however, there are clearly times during the final merger stages when the contributions are comparable. Resolving these issues requires detailed, time-dependent radiative transfer solutions through high-resolution simulations that properly sample the merger and quiescent galaxy parameter space at each redshift, and is outside the scope of this work (although an important subject for future, more detailed study; see, e.g. Li et al. 2008; Narayanan et al. 2009a,b; Younger et al. 2009a). It would be a mistake, therefore, to read too much into, for example, the detailed predictions for submillimetre galaxies or other extreme populations in Fig. 2 that may have complex dust geometries and/or a non-trivial mix of contributions from all of 'normal' and 'burst' mode star formation as well as AGN. However, most of our predicted qualitative trends, including the evolution of the luminosity density (and approximate relative contribution of mergers) and the shift in where quiescent or merger-driven populations dominate the bright IR LF, should be robust.

ACKNOWLEDGMENTS

We thank Eliot Quataert, Lin Yan, Dave Sanders, Nick Scoville and Kevin Bundy for helpful discussions throughout the development of this manuscript. Support for PFH was provided by the Miller Institute for Basic Research in Science, University of California Berkeley. JDY acknowledges support from NASA through Hubble Fellowship grant HF-51266.01 awarded by the Space Telescope Science Institute, which is operated by the Association of Universities for Research in Astronomy, Inc., for NASA, under contract NAS 5-26555. Many of the computations in this paper were run on the Odyssey cluster supported by the FAS Research Computing Group at Harvard University.

REFERENCES

Aird J. et al., 2010, MNRAS, in press (arXiv:0910.1141, doi:10.1111/j.1365-2966.2009.15829.x)
Akiyama M., Minowa Y., Kobayashi N., Ohta K., Ando M., Iwata I., 2008, ApJS, 175, 1
Alexander D. M. et al., 2008, ApJ, 687, 835
Allen P. D., Driver S. P., Graham A. W., Cameron E., Liske J., de Propris R., 2006, MNRAS, 371, 2
Arnouts S. et al., 2007, A&A, 476, 137
Austermann J. E. et al., 2010, MNRAS, 401, 160
Babbedge T. S. R. et al., 2006, MNRAS, 370, 1159
Barden M. et al., 2005, ApJ, 635, 959
Barnes J. E., 1998, in Kennicutt R. C., Jr, Schweizer F., Barnes J. E., Friedli D., Martinet L., Pfenniger D., eds, Saas-Fee Advanced Course 26: Galaxies: Interactions and Induced Star Formation. Springer-Verlag, Berlin, p. 275
Barnes J. E., Hernquist L. E., 1991, ApJ, 370, L65
Barnes J. E., Hernquist L., 1996, ApJ, 471, 115
Baugh C. M., Lacey C. G., Frenk C. S., Granato G. L., Silva L., Bressan A., Benson A. J., Cole S., 2005, MNRAS, 356, 1191
Bell E. F., de Jong R. S., 2000, MNRAS, 312, 497
Bell E. F., de Jong R. S., 2001, ApJ, 550, 212
Bell E. F., McIntosh D. H., Katz N., Weinberg M. D., 2003, ApJS, 149, 289
Bell E. F. et al., 2005, ApJ, 625, 23
Blain A. W., Jameson A., Smail I., Longair M. S., Kneib J.-P., Ivison R. J., 1999, MNRAS, 309, 715
Bluck A. F. L., Conselice C. J., Bouwens R. J., Daddi E., Dickinson M., Papovich C., Yan H., 2009, MNRAS, 394, L51
Bonoli S., Marulli F., Springel V., White S. D. M., Branchini E., Moscardini L., 2009, MNRAS, 396, 423
Borch A. et al., 2006, A&A, 453, 869
Bouché N. et al., 2007, ApJ, 671, 303
Boylan-Kolchin M., Ma C.-P., Quataert E., 2008, MNRAS, 383, 93
Bridge C. R. et al., 2007, ApJ, 659, 931
Brinchmann J. et al., 1998, ApJ, 499, 112
Brown M. J. I. et al., 2006, ApJ, 638, 88
Brown M. J. I., Dey A., Jannuzi B. T., Brand K., Benson A. J., Brodwin M., Croton D. J., Eisenhardt P. R., 2007, ApJ, 654, 858
Buat V., Burgarella D., 1998, A&A, 334, 772
Bundy K., Ellis R. S., Conselice C. J., 2005, ApJ, 625, 621
Bundy K., Fukugita M., Ellis R. S., Targett T. A., Belli S., Kodama T., 2009, ApJ, 697, 1369
Burkert A., Naab T., Johansson P. H., Jesseit R., 2008, ApJ, 685, 897
Bussmann R. S. et al., 2009a, ApJ, 693, 750
Bussmann R. S. et al., 2009b, ApJ, 705, 184
Caccianiga A. et al., 2008, A&A, 477, 735
Calura F., Jimenez R., Panter B., Matteucci F., Heavens A. F., 2008, ApJ, 682, 252

Canalizo G., Stockton A., 2001, ApJ, 555, 719
Caputi K. I. et al., 2007, ApJ, 660, 97
Casey C. M. et al., 2009, MNRAS, 399, 121
Chabrier G., 2003, PASP, 115, 763
Chapman S. C., Blain A. W., Smail I., Ivison R. J., 2005, ApJ, 622, 772
Chapman S. C., Blain A., Ibata R., Ivison R. J., Smail I., Morrison G., 2009, AJ, 691, 560
Chary R., Elbaz D., 2001, ApJ, 556, 562
Conroy C., Wechsler R. H., 2009, ApJ, 696, 620
Conselice C. J., Yang C., Bluck A. F. L., 2009, MNRAS, 394, 1956
Courteau S., Dutton A. A., van den Bosch F. C., MacArthur L. A., Dekel A., McIntosh D. H., Dale D. A., 2007, ApJ, 671, 203
Cox T. J., Dutta S. N., Di Matteo T., Hernquist L., Hopkins P. F., Robertson B., Springel V., 2006, ApJ, 650, 791
Cox T. J., Jonsson P., Somerville R. S., Primack J. R., Dekel A., 2008, MNRAS, 384, 386
Cresci G. et al., 2009, ApJ, 697, 115
Croom S. M. et al., 2009, MNRAS, 399, 1755
Daddi E. et al., 2007, ApJ, 670, 173
Dale D. A., Helou G., 2002, ApJ, 576, 159
Dasyra K. M. et al., 2006, ApJ, 638, 745
Dasyra K. M. et al., 2007, ApJ, 657, 102
Dasyra K. M., Yan L., Helou G., Surace J., Sajina A., Colbert J., 2008, ApJ, 680, 232
Davé R., 2008, MNRAS, 385, 147
Dey A. et al., 2008, ApJ, 677, 943
di Matteo P., Combes F., Melchior A.-L., Semelin B., 2007, A&A, 468, 61
Di Matteo T., Springel V., Hernquist L., 2005, Nat, 433, 604
Doyon R., Wells M., Wright G. S., Joseph R. D., Nadeau D., James P. A., 1994, ApJ, 437, L23
Driver S. P., Allen P. D., Liske J., Graham A. W., 2007, ApJ, 657, L85
Dunlop J. S., McLure R. J., Kukula M. J., Baum S. A., O'Dea C. P., Hughes D. H., 2003, MNRAS, 340, 1095
Elvis M. et al., 1994, ApJS, 95, 1
Erb D. K., 2008, ApJ, 674, 151
Erb D. K., Steidel C. C., Shapley A. E., Pettini M., Reddy N. A., Adelberger K. L., 2006, ApJ, 646, 107
Evans D. A. et al., 2009, ApJ, submitted
Fakhouri O., Ma C.-P., 2008, MNRAS, 386, 577
Fan X. et al., 2004, AJ, 128, 515
Farrah D., Afonso J., Efstathiou A., Rowan-Robinson M., Fox M., Clements D., 2003, MNRAS, 343, 585
Faucher-Giguère C.-A., Lidz A., Hernquist L., Zaldarriaga M., 2008, ApJ, 688, 85
Ferguson H. C. et al., 2004, ApJ, 600, L107
Ferrarese L., Merritt D., 2000, ApJ, 539, L9
Fisher D. B., 2006, ApJ, 642, L17
Fisher D. B., Drory N., 2008, AJ, 136, 773
Floyd D. J. E., Kukula M. J., Dunlop J. S., McLure R. J., Miller L., Percival W. J., Baum S. A., O'Dea C. P., 2004, MNRAS, 355, 196
Fontana A. et al., 2006, A&A, 459, 745
Fontanot F., De Lucia G., Monaco P., Somerville R. S., Santini P., 2009, MNRAS, 397, 1776
Foreman G., Volonteri M., Dotti M., 2009, ApJ, 693, 1554
Förster Schreiber N. M. et al., 2009, ApJ, 706, 1364
Foster C., Proctor R. N., Forbes D. A., Spolaor M., Hopkins P. F., Brodie J. P., 2009, MNRAS, 400, 2135
Franceschini A. et al., 2005, AJ, 129, 2074
Franceschini A. et al., 2006, A&A, 453, 397
Gebhardt K. et al., 2000, ApJ, 539, L13
Genzel R., Tacconi L. J., Rigopoulou D., Lutz D., Tecza M., 2001, ApJ, 563, 527
Gilli R., Comastri A., Hasinger G., 2007, A&A, 463, 79
Guyon O., Sanders D. B., Stockton A., 2006, ApJS, 166, 89
Hasinger G., 2008, A&A, 490, 905
Hernquist L., Spergel D. N., Heyl J. S., 1993, ApJ, 416, 415
Hickox R. C. et al., 2007, ApJ, 671, 1365
Hopkins A. M., 2004, ApJ, 615, 209
Hopkins A. M., Beacom J. F., 2006, ApJ, 651, 142
Hopkins P. F., Hernquist L., 2006, ApJS, 166, 1
Hopkins P. F., Hernquist L., 2009a, ApJ, 694, 599
Hopkins P. F., Hernquist L., 2009b, ApJ, 698, 1550
Hopkins P. F., Hernquist L., Cox T. J., Di Matteo T., Martini P., Robertson B., Springel V., 2005a, ApJ, 630, 705
Hopkins P. F., Hernquist L., Cox T. J., Di Matteo T., Robertson B., Springel V., 2005b, ApJ, 630, 716
Hopkins P. F., Hernquist L., Cox T. J., Di Matteo T., Robertson B., Springel V., 2005c, ApJ, 632, 81
Hopkins P. F., Hernquist L., Martini P., Cox T. J., Robertson B., Di Matteo T., Springel V., 2005d, ApJ, 625, L71
Hopkins P. F., Hernquist L., Cox T. J., Di Matteo T., Robertson B., Springel V., 2006a, ApJS, 163, 1
Hopkins P. F., Hernquist L., Cox T. J., Robertson B., Di Matteo T., Springel V., 2006b, ApJ, 639, 700
Hopkins P. F., Somerville R. S., Hernquist L., Cox T. J., Robertson B., Li Y., 2006c, ApJ, 652, 864
Hopkins P. F., Hernquist L., Cox T. J., Robertson B., Krause E., 2007a, ApJ, 669, 45
Hopkins P. F., Hernquist L., Cox T. J., Robertson B., Krause E., 2007b, ApJ, 669, 67
Hopkins P. F., Richards G. T., Hernquist L., 2007c, ApJ, 654, 731
Hopkins P. F., Cox T. J., Hernquist L., 2008a, ApJ, 689, 17
Hopkins P. F., Cox T. J., Kereš D., Hernquist L., 2008b, ApJS, 175, 390
Hopkins P. F., Hernquist L., Cox T. J., Dutta S. N., Rothberg B., 2008c, ApJ, 679, 156
Hopkins P. F., Hernquist L., Cox T. J., Kereš D., 2008d, ApJS, 175, 356
Hopkins P. F., Cox T. J., Dutta S. N., Hernquist L., Kormendy J., Lauer T. R., 2009a, ApJS, 181, 135
Hopkins P. F., Cox T. J., Younger J. D., Hernquist L., 2009b, ApJ, 691, 1168
Hopkins P. F., Hernquist L., Cox T. J., Kereš D., Wuyts S., 2009c, ApJ, 691, 1424
Hopkins P. F., Hickox R., Quataert E., Hernquist L., 2009d, MNRAS, 398, 333
Hopkins P. F., Lauer T. R., Cox T. J., Hernquist L., Kormendy J., 2009e, ApJS, 181, 486
Hopkins P. F. et al., 2009f, MNRAS, 397, 802
Hopkins P. F. et al. 2009g, MNRAS, in press (arXiv:0906.5357)
Huang J.-S. et al., 2007, ApJ, 664, 840
Hutchings J. B., Cherniawsky A., Cutri R. M., Nelson B. O., 2006, AJ, 131, 680
Ilbert O. et al., 2009, ApJ, in press (arXiv:0903.0102)
James P., Bate C., Wells M., Wright G., Doyon R., 1999, MNRAS, 309, 585
Jesseit R., Cappellari M., Naab T., Emsellem E., Burkert A., 2009, MNRAS, 397, 1202
Jogee S., 2006, in Alloin D., ed., Lecture Notes in Physics, Vol. 693, Physics of Active Galactic Nuclei at All Scales. Springer-Verlag, Berlin, p. 143
Jogee S. et al., 2009, ApJ, 697, 1971
Jonsson P., Cox T. J., Primack J. R., Somerville R. S., 2006, ApJ, 637, 255
Joseph R. D., 1999, Ap&SS, 266, 321
Joseph R. D., Wright G. S., 1985, MNRAS, 214, 87
Kajisawa M. et al., 2009, ApJ, 702, 1393
Kartaltepe J. S. et al., 2007, ApJS, 172, 320
Kauffmann G. et al., 2003, MNRAS, 346, 1055
Kennicutt R. C., Jr, 1998, ApJ, 498, 541
Kereš D., Katz N., Weinberg D. H., Davé R., 2005, MNRAS, 363, 2
Kereš D., Katz N., Fardal M., Davé R., Weinberg D. H., 2009, MNRAS, 395, 160
Kewley L. J., Groves B., Kauffmann G., Heckman T., 2006, MNRAS, 372, 961
Kimm T. et al., 2009, MNRAS, 394, 1131
Kormendy J., Kennicutt R. C., Jr, 2004, ARA&A, 42, 603
Kroupa P., 2002, Sci, 295, 82
Lake G., Dressler A., 1986, ApJ, 310, 605
Le Floc'h E. et al., 2005, ApJ, 632, 169
Li Y. et al., 2008, ApJ, 678, 41
Lin L. et al., 2008, ApJ, 681, 232

Lotz J. M., Jonsson P., Cox T. J., Primack J. R., 2008, MNRAS, 391, 1137
Lutz D., Spoon H. W. W., Rigopoulou D., Moorwood A. F. M., Genzel R., 1998, ApJ, 505, L103
McDermid R. M. et al., 2006, MNRAS, 373, 906
McGaugh S. S., 2005, ApJ, 632, 859
Magnelli B., Elbaz D., Chary R. R., Dickinson M., Le Borgne D., Frayer D. T., Willmer C. N. A., 2009, A&A, 496, 57
Magorrian J. et al., 1998, AJ, 115, 2285
Malizia A., Stephen J. B., Bassani L., Bird A. J., Panessa F., Ubertini P., 2009, MNRAS, 399, 944
Malkan M. A., Gorjian V., Tam R., 1998, ApJS, 117, 25
Maller A. H., Katz N., Kereš D., Davé R., Weinberg D. H., 2006, ApJ, 647, 763
Mannucci F. et al., 2009, MNRAS, 398, 1915
Marchesini D., van Dokkum P. G., Förster Schreiber N. M., Franx M., Labbé I., Wuyts S., 2009, ApJ, 701, 1765
Marulli F., Bonoli S., Branchini E., Gilli R., Moscardini L., Springel V., 2009, MNRAS, 396, 1404
Melbourne J. et al., 2008, AJ, 136, 1110
Menanteau F., Ford H. C., Motta V., Benítez N., Martel A. R., Blakeslee J. P., Infante L., 2006, AJ, 131, 208
Menéndez-Delmestre K. et al., 2009, ApJ, 699, 667
Mihos J. C., Hernquist L., 1994, ApJ, 431, L9
Mihos J. C., Hernquist L., 1996, ApJ, 464, 641
Murray N., Quataert E., Thompson T. A., 2005, ApJ, 618, 569
Naab T., Jesseit R., Burkert A., 2006, MNRAS, 372, 839
Narayanan D., Cox T. J., Hayward C., Younger J. D., Hernquist L., 2009a, ApJ, in press (arXiv:0905.2184)
Narayanan D., Hayward C. C., Cox T. J., Hernquist L., Jonsson P., Younger J. D., Groves B., 2009b, ApJ, in press (arXiv:0904.0004)
Nardini E., Risaliti G., Salvati M., Sani E., Watabe Y., Marconi A., Maiolino R., 2009, MNRAS, 399, 1373
Natarajan P., Treister E., 2009, MNRAS, 393, 838
Nayakshin S., King A., 2007, MNRAS, submitted (arXiv:0705.1686)
Noeske K. G. et al. 2007a, ApJ, 660, L47
Noeske K. G. et al. 2007b, ApJ, 660, L43
Novak G. S., Faber S. M., Dekel A., 2006, ApJ, 637, 96
Pannella M., Hopp U., Saglia R. P., Bender R., Drory N., Salvato M., Gabasch A., Feulner G., 2006, ApJ, 639, L1
Papovich C., Dickinson M., Giavalisco M., Conselice C. J., Ferguson H. C., 2005, ApJ, 631, 101
Papovich C. et al., 2006, ApJ, 640, 92
Peng C. Y., Impey C. D., Rix H.-W., Kochanek C. S., Keeton C. R., Falco E. E., Lehár J., McLeod B. A., 2006, ApJ, 649, 616
Pérez-González P. G. et al., 2005, ApJ, 630, 82
Pérez-González P. G. et al., 2008, ApJ, 675, 234
Polletta M. d. C. et al., 2006, ApJ, 642, 673
Pope A. et al., 2008a, ApJ, 675, 1171
Pope A. et al, 2008b, ApJ, 689, 127
Puech M. et al., 2008, A&A, 484, 173
Ravindranath S. et al., 2004, ApJ, 604, L9
Reda F. M., Proctor R. N., Forbes D. A., Hau G. K. T., Larsen S. S., 2007, MNRAS, 377, 1772
Richards G. T. et al, 2006a, ApJS, 166, 470
Richards G. T. et al, 2006b, AJ, 131, 2766
Rigby J. R., Rieke G. H., Donley J. L., Alonso-Herrero A., Pérez-González P. G., 2006, ApJ, 645, 115
Robaina A. R. et al., 2009, ApJ, 704, 324
Robertson B., Cox T. J., Hernquist L., Franx M., Hopkins P. F., Martini P., Springel V., 2006, ApJ, 641, 21
Rothberg B., Joseph R. D., 2004, AJ, 128, 2098
Rothberg B., Joseph R. D., 2006, AJ, 131, 185
Sajina A., Yan L., Armus L., Choi P., Fadda D., Helou G., Spoon H., 2007, ApJ, 664, 713
Salpeter E. E., 1955, ApJ, 121, 161
Salviander S., Shields G. A., Gebhardt K., Bonning E. W., 2007, ApJ, 662, 131
Sánchez-Blázquez P., Forbes D. A., Strader J., Brodie J., Proctor R., 2007, MNRAS, 377, 759
Sanders D. B., 1999, Ap&SS, 266, 331
Sanders D. B., Mirabel I. F., 1996, ARA&A, 34, 749
Sanders D. B., Soifer B. T., Elias J. H., Madore B. F., Matthews K., Neugebauer G., Scoville N. Z., 1988a, ApJ, 325, 74
Sanders D. B., Soifer B. T., Elias J. H., Neugebauer G., Matthews K., 1988b, ApJ, 328, L35
Sargent A. I., Sanders D. B., Scoville N. Z., Soifer B. T., 1987, ApJ, 312, L35
Saunders W., Rowan-Robinson M., Lawrence A., Efstathiou G., Kaiser N., Ellis R. S., Frenk C. S., 1990, MNRAS, 242, 318
Scalo J. M., 1986, Fundam. Cosmic Phys., 11, 1
Schinnerer E. et al., 2008, ApJ, 689, L5
Scoville N. Z., Sanders D. B., Sargent A. I., Soifer B. T., Scott S. L., Lo K. Y., 1986, ApJ, 311, L47
Shankar F., 2009, New Astron. Rev., 53, 57
Shankar F., Weinberg D. H., Miralda-Escudé J., 2009, ApJ, 690, 20
Shapley A. E., Coil A. L., Ma C.-P., Bundy K., 2005, ApJ, 635, 1006
Shen S., Mo H. J., White S. D. M., Blanton M. R., Kauffmann G., Voges W., Brinkmann J., Csabai I., 2003, MNRAS, 343, 978
Shi Y. et al., 2006, ApJ, 653, 127
Shier L. M., Fischer J., 1998, ApJ, 497, 163
Shlosman I., Frank J., Begelman M. C., 1989, Nat, 338, 45
Silk J., Rees M. J., 1998, A&A, 331, L1
Soifer B. T., Neugebauer G., 1991, AJ, 101, 354
Soifer B. T. et al., 1984, ApJ, 283, L1
Soifer B. T., Sanders D. B., Madore B. F., Neugebauer G., Danielson G. E., Elias J. H., Lonsdale C. J., Rice W. L., 1987, ApJ, 320, 238
Solomon P. M., Downes D., Radford S. J. E., Barrett J. W., 1997, ApJ, 478, 144
Soltan A., 1982, MNRAS, 200, 115
Somerville R. S. et al., 2008, ApJ, 672, 776
Springel V., Di Matteo T., Hernquist L., 2005a, ApJ, 620, L79
Springel V. et al, 2005b, Nat, 435, 629
Swinbank A. M. et al., 2008, MNRAS, 391, 420
Tacconi L. J., Genzel R., Lutz D., Rigopoulou D., Baker A. J., Iserlohe C., Tecza M., 2002, ApJ, 580, 73
Tacconi L. J. et al., 2006, ApJ, 640, 228
Tacconi L. J. et al., 2008, ApJ, 680, 246
Tajer M. et al., 2007, A&A, 467, 73
Toft S. et al., 2007, ApJ, 671, 285
Treister E., Urry C. M., 2006, ApJ, 652, L79
Treister E., Krolik J. H., Dullemond C., 2008, ApJ, 679, 140
Treister E., Urry C. M., Virani S., 2009, ApJ, 696, 110
Treu T., Woo J.-H., Malkan M. A., Blandford R. D., 2007, ApJ, 667, 117
Trichas M., Georgakakis A., Rowan-Robinson M., Nandra K., Clements D., Vaccari M., 2009, MNRAS, 399, 663
Trujillo I. et al., 2004, ApJ, 604, 521
Ueda Y., Akiyama M., Ohta K., Miyaji T., 2003, ApJ, 598, 886
Urrutia T., Lacy M., Becker R. H., 2008, ApJ, 674, 80
Valiante E., Lutz D., Sturm E., Genzel R., Chapin E. L., 2009, ApJ, 701, 1814
Veilleux S. et al, 2009a, ApJ, 701, 587
Veilleux S. et al, 2009b, ApJS, 182, 628
Volonteri M., Salvaterra R., Haardt F., 2006, MNRAS, 373, 121
Watabe Y., Risaliti G., Salvati M., Nardini E., Sani E., Marconi A., 2009, MNRAS, 396, L1
Weinmann S. M., van den Bosch F. C., Yang X., Mo H. J., Croton D. J., Moore B., 2006, MNRAS, 372, 1161
Woo J.-H., Treu T., Malkan M. A., Blandford R. D., 2006, ApJ, 645, 900
Yan L. et al., 2007, ApJ, 658, 778
Yang M., Greve T. R., Dowell C. D., Borys C., 2007, ApJ, 660, 1198
Yencho B., Barger A. J., Trouille L., Winter L. M., 2009, ApJ, 698, 380
Younger J. D. et al., 2007, ApJ, 671, 1531
Younger J. D., Hopkins P. F., Cox T. J., Hernquist L., 2008a, ApJ, 686, 815
Younger J. D. et al, 2008b, ApJ, 688, 59

Younger J. D., Hayward C. C., Narayanan D., Cox T. J., Hernquist L., Jonsson P., 2009a, MNRAS, 396, L66
Younger J. D. et al., 2009b, MNRAS, 394, 1685
Younger J. D. et al., 2009c, ApJ, 704, 803
Yun M. S., Reddy N. A., Condon J. J., 2001, ApJ, 554, 803
Zakamska N. L., Strauss M. A., Heckman T. M., Ivezić, Ž., Krolik J. H., 2004, AJ, 128, 1002
Zakamska N. L. et al., 2006, AJ, 132, 1496
Zakamska N. L., Gómez L., Strauss M. A., Krolik J. H., 2008, AJ, 136, 1607

APPENDIX A: PREDICTED LUMINOSITY FUNCTIONS AS A FUNCTION OF WAVELENGTH

Fig. 2 presents the predicted total IR LFs from the models discussed here. To facilitate comparison with observations (and broaden the range of observations to which we can compare), we here present corresponding predictions in a number of different rest-frame wavelengths. Figs A1–A5 present the predicted LFs at rest-frame wavelengths of 8, 24, 60, 100 and 160 μm, respectively. For each, we compare to the available observations at or near that wavelength.

For the star-forming systems (normal galaxies and mergers), we simply convert our predicted SFR and corresponding total IR luminosity to an observed luminosity in the given band, given the SED templates (themselves a function of bolometric luminosity) discussed in Section 3.1, namely those from Valiante et al. (2009), using the model SEDs in Dale & Helou (2002). As discussed in Section 3, varying the exact scaling of these corrections within observational uncertainties is comparable to the uncertainty from adopting different MF estimators. For the AGN, we adopt the template SEDs for obscured and unobscured systems from Hopkins et al. (2007c), but adopting alternative different template obscured or unobscured AGN spectra (e.g. those in Elvis et al. 1994; Zakamska et al. 2004; Polletta et al. 2006; Richards et al. 2006a) makes little difference.

We stress that these predictions should be regarded with considerable caution. The models here (or, for that matter, in any fully cosmological model for disc/merger/AGN systems as a function of redshift) do *not* predict full SEDs. Rather, the robust quantity is some more physical number such as the total SFR (or AGN luminosity and obscured fraction). This allows robust estimations of total IR luminosity, but we are now using a specific, simple empirical conversion between bolometric luminosity and luminosity at a given wavelength. If structural properties of galaxies, spatial distributions of gas and star formation, dust properties (gas-to-dust ratios, dust spatial distributions and clumpiness), clumping factors and AGN contributions evolve, then these conversions will be problematic and may introduce systematic errors. In fact, it is very likely that these parameters that govern the SED do, in fact, evolve with redshift, or are different in merging and non-merging systems (given the different spatial distributions of gas and dust), and/or are a function of the relative AGN/star formation balance in the galaxy.

More detailed modelling, including full, self-consistent radiative transfer treatment of high-resolution hydrodynamic simulations of mergers and normal galaxies with all the effects above included, will be necessary to predict, for example, the distribution of dust

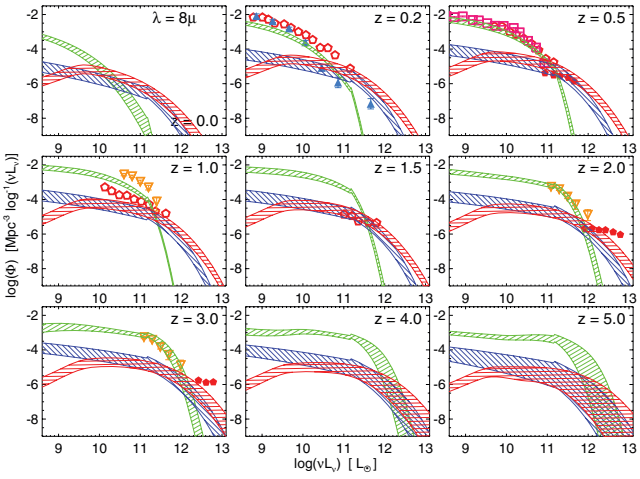

Figure A1. As Fig. 2, but for the LF in a specific rest-frame band (here, λ = 8 μm) as a function of redshift. We stress that we do *not* model the SEDs a priori, but simply adopt a specific set of empirical templates – as such, the information in this plot is identical to that in Fig. 2. We compare to the same observations as Fig. 2, for the observations at or near this rest-frame wavelength. Solid red pentagons show the estimates from Babbedge et al. (2006) specifically for the contribution of AGN at this wavelength.

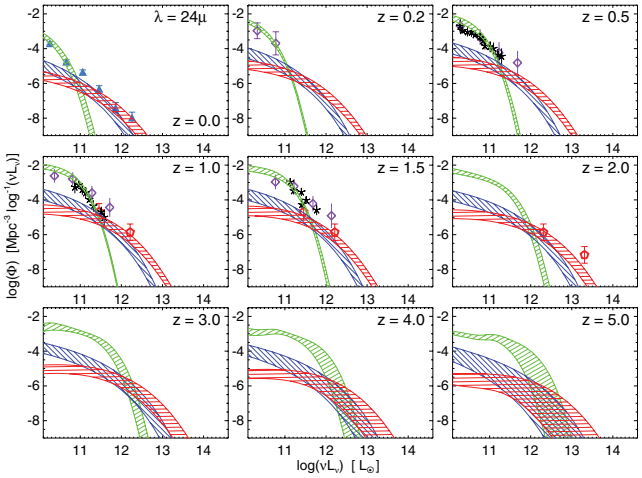

Figure A2. As Fig. A1, but at rest-frame 24 μm. We compare observations spanning rest-frame 15−35 μm (corrected with the same standard bolometric corrections to 24 μm).

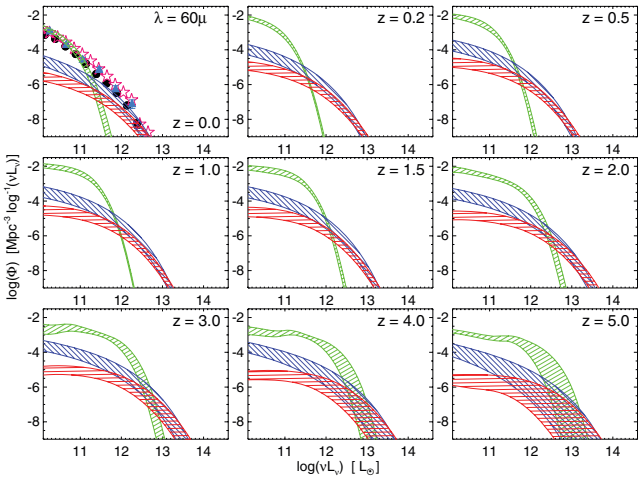

Figure A3. As Fig. A1, but at rest-frame 60 μm. We compare observations spanning rest-frame 60–70 μm (corrected with the same standard bolometric corrections to 60 μm).

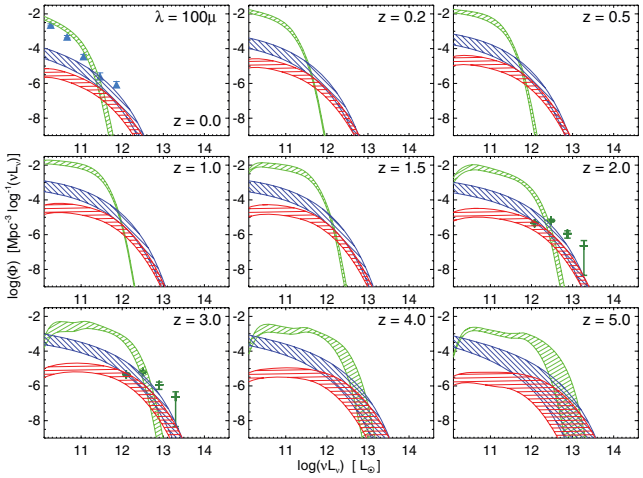

Figure A4. As Fig. A1, but at rest-frame 100 μm. We compare observations spanning rest-frame 80–120 μm (corrected with the same standard bolometric corrections to 100 μm).

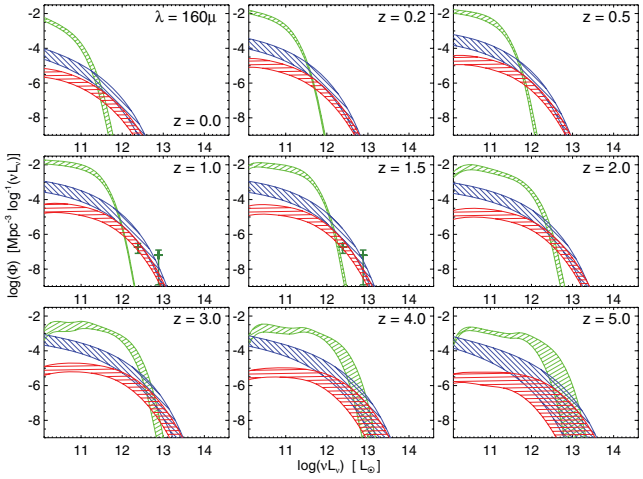

Figure A5. As Fig. A1, but at rest-frame 160 μm. We compare observations spanning rest-frame 120–350 μm (corrected with the same standard bolometric corrections to 160 μm).

temperatures and other quantities critical, especially, for comparison with the number counts at long wavelengths (e.g. sub-millimetre galaxies). These models will be presented in a future work (in preparation); therefore, we do not construct such comparisons (or attempt to compile predicted number counts) here.

Nevertheless, the comparisons in Figs A1–A5 are informative, and useful for future comparisons with observations, provided appropriate caution is used. In particular, this allows us to see how the relative contributions of AGN and star formation vary as a function of IR wavelength (as the dust temperatures and SEDs are not the same). At shorter wavelengths, e.g. 8 μm, AGN play a role at even moderate luminosities. We can compare to some observational studies, for example that in Babbedge et al. (2006), that explicitly separate the AGN and star-forming populations, and find a good agreement. On the other hand, at the longest wavelengths, the warmer dust temperatures typical in AGN lead to their being relatively less important.

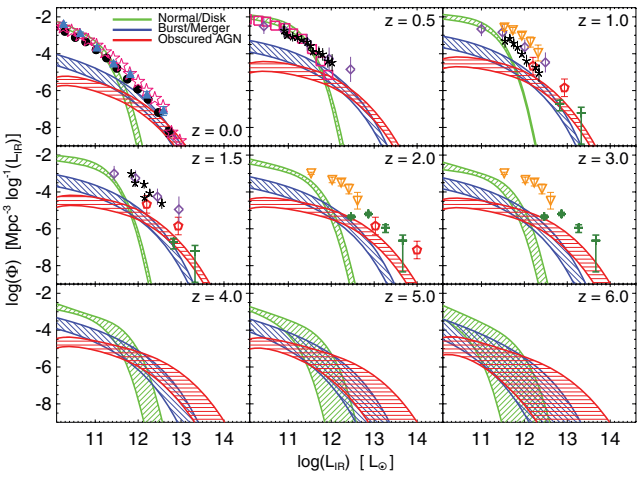

Figure B1. As Fig. 2, but neglecting the increase in galaxy gas fractions with redshift. The SFRs of even normal, low-mass undisturbed discs are significantly underpredicted.

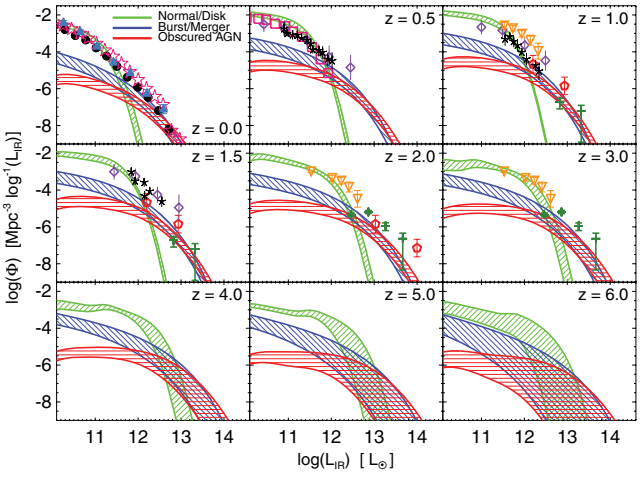

Figure B2. As Fig. 2, but neglecting the evolution in disc sizes with redshift. Because the observed size evolution (of star-forming galaxies) is relative weak [$R_e(M_*) \propto (1+z)^{-(0-0.6)}$] and the size evolution (at otherwise fixed properties) only enters into the SFR at sublinear order, the difference is relatively small (a factor of ∼2).

APPENDIX B: CONSEQUENCES OF MODEL ASSUMPTIONS

The consequences of adding, removing, or changing some of our model assumptions are discussed in Section 3.5. Here, in Figs B1–B4, we explicitly illustrate the effects discussed there.

In Fig. B1, we reproduce Fig. 2, but do not allow galaxy gas fractions to evolve with redshift (adopting the $z = 0$ value at all redshifts). As discussed in Section 3.5, this leads to significant underprediction of the IR LF at high redshifts. In Fig. B2, we reproduce Fig. 2 again, but this time do not allow for disc sizes to be more compact at high redshift. This has a much smaller effect. In Fig. B3, we repeat Fig. 2 but do not allow for scatter in any quantities (e.g. disc sizes, gas fractions, burst masses, quasar bolometric corrections and SFRs at otherwise fixed properties); i.e. all values exactly trace the medians given in Section 2. This suppresses the

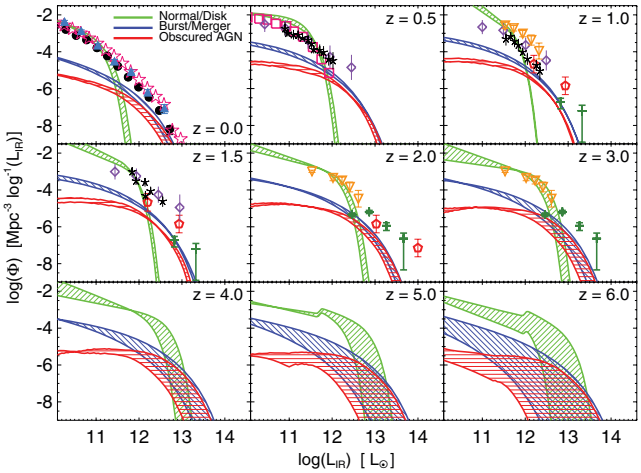

Figure B3. As Fig. 2, but not allowing for any scatter in SFR at fixed galaxy mass, in mergers or discs (and no scatter in obscured fractions/bolometric corrections in AGN). The high-L tail is significantly suppressed. Note that the 'kinks' at high redshift are artefacts of the analytic fitting functions used.

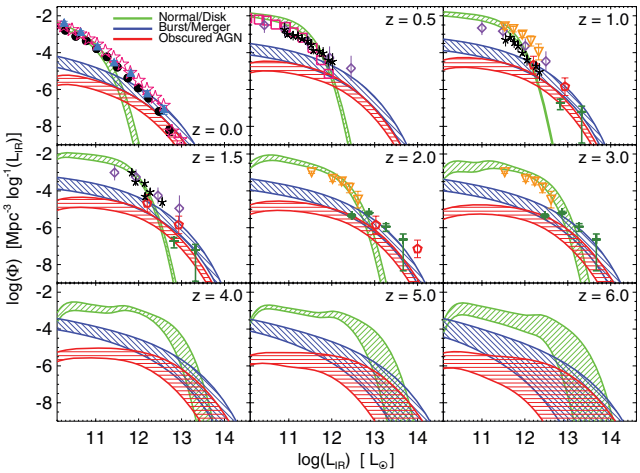

Figure B4. As Fig. 2, but with all calculations adopting a steeper index in the Kennicutt relation (equation 3), $n_s = 1.6$, normalized to the same SFR for Milky Way like discs. Systems at high redshifts are boosted significantly in SFR, and mergers are more concentrated in time, leading to sharper peak SFRs. The agreement with observations is somewhat improved, but overall the differences are comparable to the uncertainties from the adopted SFR.

bright end of the LF. In Fig. B4, we repeat Fig. 2, but adopt a steeper power-law index for the Kennicutt (1998) relation ($\dot{\Sigma}_* \propto \Sigma_{\rm gas}^{1.6}$) (as discussed in Section 3.5). These LFs correspond to the fits for the steep Kennicutt–Schmidt slope case presented in Table 1.

This paper has been typeset from a TEX/LATEX file prepared by the author.